AD-A154 441 ELECTRON IRRADIATION OF LIGHT EMITTING DIODES(U) NAVAL POSTGRADUATE SCHOOL MONTEREY CA C Q NESS DEC 84 1/2

UNCLASSIFIED F/G 9/1 NL

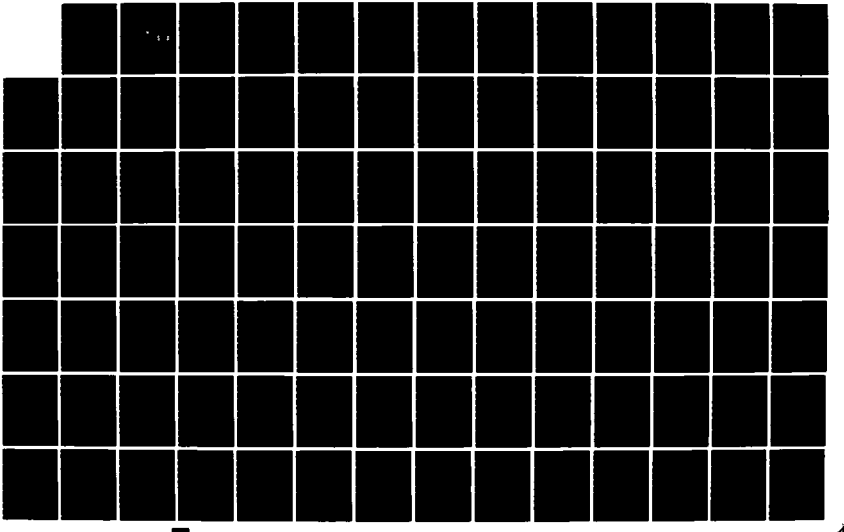

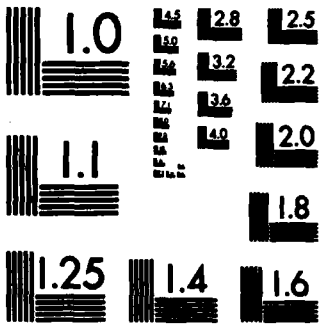

NAVAL POSTGRADUATE SCHOOL
Monterey, California

THESIS

ELECTRON IRRADIATION OF LIGHT EMITTING DIODES

by

Christian Quarles Ness

December 1984

Thesis Advisor: K.C. Dimiduk

Approved for public release; distribution is unlimited

SECURITY CLASSIFICATION OF THIS PAGE *(When Data Entered)*

REPORT DOCUMENTATION PAGE

READ INSTRUCTIONS BEFORE COMPLETING FORM

1. REPORT NUMBER	2. GOVT ACCESSION NO. / 3. RECIPIENT'S CATALOG NUMBER
4. TITLE *(and Subtitle)*: Electron Irradiation of Light Emitting Diodes	5. TYPE OF REPORT & PERIOD COVERED: Master's Thesis; December 1984
	6. PERFORMING ORG. REPORT NUMBER
7. AUTHOR(s): Christian Quarles Ness	8. CONTRACT OR GRANT NUMBER(s)
9. PERFORMING ORGANIZATION NAME AND ADDRESS: Naval Postgraduate School, Monterey, California 93943	10. PROGRAM ELEMENT, PROJECT, TASK AREA & WORK UNIT NUMBERS
11. CONTROLLING OFFICE NAME AND ADDRESS: Naval Postgraduate School, Monterey, California 93943	12. REPORT DATE: December 1984
	13. NUMBER OF PAGES: 96 pages
14. MONITORING AGENCY NAME & ADDRESS *(if different from Controlling Office)*	15. SECURITY CLASS. *(of this report)*: Unclassified
	15a. DECLASSIFICATION/DOWNGRADING SCHEDULE

16. DISTRIBUTION STATEMENT *(of this Report)*

Approved for public release; distribution is unlimited

17. DISTRIBUTION STATEMENT *(of the abstract entered in Block 20, if different from Report)*

18. SUPPLEMENTARY NOTES

(20)

19. KEY WORDS *(Continue on reverse side if necessary and identify by block number)*

electron irradiation, light emitting diodes, LEDs, radiation effects, liquid phase epitaxy, vapor phase epitaxy, LPE, VPE, GaAs, GaP, $GaAs_xP_{(1-x)}$

20. ABSTRACT *(Continue on reverse side if necessary and identify by block number)*

An experiment is described in which 30-MeV electrons were used to irradiate LEDs. A brief description of typical electron radiation sources is given along with a description of the effects of electron radiation on semiconductors. Using a simple model for LED current generation, a set of equations for determining phenomenological damage constants is given. The damage sustained by the LEDs increased total current

DD FORM 1 JAN 73 1473 EDITION OF 1 NOV 65 IS OBSOLETE

S/N 0102-LF-014-6601

SECURITY CLASSIFICATION OF THIS PAGE *(When Data Entered)*

20. (Continued)

but reduced radiative current for a given voltage and was similar to that seen by earlier workers performing comparable experiments with electrons, protons, and neutrons. Four groups of LEDs were studied. The group of LEDs fabricated by liquid phase epitaxy (LPE) had an average lifetime-damage constant product $\tau_0 K = 6.4 \times 10^{-13}$ cm^2/e^- which was much greater than the averages for three different color groups of LEDs fabricated by vapor phase epitaxy (VPE) where the average lifetime-damage constant products were $\tau_0 K = 1.3 \times 10^{-13}$ cm^2/e^-, $\tau_0 K = 0.7 \times 10^{-13}$ cm^2/e^- and $\tau_0 K = 1.9 \times 10^{-13}$ cm^2/e^-. This indicated that the LPE devices are from 3 to 9 times as susceptible to damage as the VPE devices.

keywords included

Approved for public release; distribution is unlimited

Electron Irradiation of Light Emitting Diodes

by

Christian Quarles Ness
Lieutenant Commander, United States Navy
B.S., United States Naval Academy, 1972

Submitted in partial fulfillment of the
requirements for the degree of

MASTER OF SCIENCE IN PHYSICS

from the

NAVAL POSTGRADUATE SCHOOL
December 1984

Author: _____
Christian Quarles Ness

Approved by: _____
K. C. Dimiduk, Thesis Advisor

_____
H. E. Handler, Second Reader

_____
G. E. Schacher, Chairman, Department of Physics

_____
J. N. Dyer, Dean of Science and Engineering

ABSTRACT

An experiment is described in which 30-MeV electrons were used to irradiate LEDs. A brief description of typical electron radiation sources is given along with a description of the effects of electron radiation on semiconductors. Using a simple model for LED current generation, a set of equations for determining phenomenological damage constants is given. The damage sustained by the LEDs increased total current but reduced radiative current for a given voltage and was similar to that seen by earlier workers performing comparable experiments with electrons, protons, and neutrons. Four groups of LEDs were studied. The group of LEDs fabricated by liquid phase epitaxy (LPE) had an average lifetime-damage constant product $\tau_0 K = 6.4 \times 10^{-13}$ cm^2/e^- which was much greater than the averages for three different color groups of LEDs fabricated by vapor phase epitaxy (VPE) where the average lifetime-damage constant products were $\tau_0 K = 1.3 \times 10^{-13}$ cm^2/e^-, $\tau_0 K = 0.7 \times 10^{-13}$ cm^2/e^- and $\tau_0 K = 1.9 \times 10^{-13}$ cm^2/e^-. This indicated that the LPE devices are from 3 to 9 times as susceptible to damage as the VPE devices.

TABLE OF CONTENTS

ACKNOWLEDGEMENT

The completion of this work owes much to the continuous encouragement of my advisor, Dr. Kathryn C. Dimiduk. Her patience in working with me was invaluable as was her expertise in answering my many questions.

I also thank Don Snyder for working at the LINAC control station for many long hours and providing the know how to get the job done. Another who deserves thanks is Andy Smith of NSWC and NPS teaching fame, whose undiminished enthusiasm for this type of work laid the groundwork for my knowledge and interest in this area.

The Hewlett Packard Optoelectronics Division deserves appreciation for providing the LEDs, lens cap and plastic material samples. Naval Surface Weapons Center and the Naval Postgraduate School Foundation Research Program earn special thanks for providing funding for the project.

I. INTRODUCTION

A. OVERVIEW

Optoelectronic components and devices are used extensively in communications and control systems in satellites and tactical military systems. The outer space environment and nuclear weapons threat possess the potential for causing radiation induced damage in these devices. This threat has led to investigations into the hardness of individual components to the various types of radiation.

While silicon is the most common material basis for semiconductor devices, other materials can have important specialized applications. GaAs and $GaAs_{1-x}P_x$ (Gallium Arsenide Phosphide where x indicates the fraction of phosphorous) are two compounds commonly used in the fabrication of semiconductor devices such as Light Emitting Diodes (LEDs). These components and the devices fabricated from them have been studied for their reactions to the various nuclear radiations. Because of its annealing properties, Gallium Arsenide (GaAs) has been proposed as the material for use in the solar panels of the NASA Solar Power Satellite (SPS) where long lifetime is needed for a device that will be exposed to the Van Allen radiation belts and to cosmic radiation [Ref. 1].

The LED is a simple semiconductor device that allows convenient measurement of its characteristics and is a good vehicle for quantifying radiation damage effects. In this work I report on the effect of electron radiation on several kinds of LEDs.

B. PREVIOUS WORK

The radiative conversion efficiency of LEDs (the ratio of the light producing current, I, to the total current, J) is reduced by ionizing radiation such as high energy electrons and protons. Gamma rays and neutrons also produce secondary effects that lead to ionization. These different categories of radiation can all cause displacement defects in a material's crystal lattice. These defects introduce additional states in a semiconductor's energy gap and can act as additional recombination centers. The additional recombination centers cause a reduction in minority carrier lifetime. Two categories of defects are possible. Simple defects, composed of at most a few atoms associated together, form a relatively stable defect. They are characteristic of electron, low energy proton, and gamma ray damage in which energy imparted to any single crystal atom is small. Cluster defects involve a large disordered region of up to several hundred atoms and are caused by neutrons and high energy protons which can impart a large amount of kinetic energy to a single atomic nucleus [Ref. 2].

Ionizing radiation can also alter device operation by introducing trapped charges into the device.

Schade and co-workers [Ref. 3] investigated the effects of electron irradiation of $GaAs_{1-x}P_x$ LEDs. They found a large decrease in the light output of diodes after irradiation. They concluded that light emission originated in the neutral p-region and the output degradation was due to the production of non-radiative recombination centers. The center primarily responsible was an acceptor. Its influence was independent of alloy composition. They also detected indications of annealing.

Stanley [Ref. 4] irradiated various types of LEDs with electrons. A dependence on the method of semiconductor fabrication for hardness levels was detected. GaAs devices made by epitaxy were more sensitive to radiation than standard diffused types. The devices in the present experiment were fabricated by liquid phase epitaxy (LPE) or vapor phase epitaxy (VPE).

Millea and Aukerman [Ref. 5 and 6] studied electron radiation effects on GaAs LEDs. They found that light intensity, I, went as:

$$I = I_o \exp(qV_a/kT) \qquad (1)$$

over several orders of magnitude at $78^{\circ}K$ and $298^{\circ}K$. I_o is initial intensity, q is the unit of charge, V_a the applied

voltage, k is the Boltzmann constant (1.38×10^{-23} J/°K) and T is the temperature in °K. This relationship can be used to determine a damage constant for the LED as shown later.

Barnes [Ref. 7] provided a good summary of work in LED irradiation with the different effects including electron, proton, and neutron induced damage. In a later paper [Ref. 8] he described an experiment using protons with a relatively high energy (16 MeV). This more recent paper confirmed much of the previous work and provided a descriptive basis for the procedures used in the present experiment.

C. PRESENT EXPERIMENT

Many different types of LEDs are available for use in optoelectronics systems. This investigation studied LEDs with one basic mechanical configuration but with varying semiconductor material compositions. The variation in composition gave four different wavelength outputs (colors) all in the visible region: red, high efficiency red (HER), green and yellow. The green LEDs were fabricated using LPE and the others using VPE.

The LEDs were irradiated with 30-MeV electrons using the Linear Accelerator (LINAC) at the Naval Postgraduate School.

The configuration of the LEDs and their operating characteristics are shown in Figure 1 and Table I which are

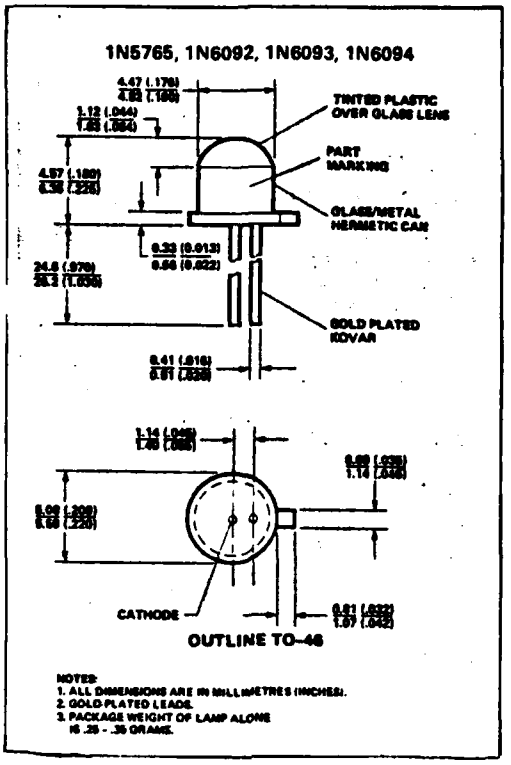

Figure 1. LED Configuration

taken from the Hewlett Packard Optoelectronics Designer's Catalog 1984. The LEDs were tested as discrete components and not part of a system. The tinted plastic and glass lenses on the top of the LEDs were removed so that radiation induced darkening of the lens would not interfere with light output measurements. Note that the catalog numbers for the LEDs correspond as follows: 1N5765 --> HLMP-0904 (Red); 1N6092 --> HLMP-0354 (HER); 1N6093 --> HLMP-0454 (yellow); 1N6094 --> HLMP-0554 (green).

TABLE I

LED PERFORMANCE SPECIFICATIONS

Absolute Maximum Ratings at T_A=25°C

Parameter	Red HLMP-0904	High Eff. Red HLMP-0354	Yellow HLMP-0454	Green HLMP-0554	Units
Power Dissipation (derate linearly from 50°C at 1.6mW/°C)	100	120	120	120	mW
DC Forward Current	50[1]	35[2]	35[2]	35[2]	mA
Peak Forward Current	1000 See Fig. 5	60 See Fig. 10	60 See Fig. 15	60 See Fig. 20	mA
Operating and Storage Temperature Range	-65°C to 100°C				
Lead Soldering Temperature [1.6mm (0.063 in.) from body]	260°C for 7 seconds.				

Notes: 1. Derate from 50°C at 0.2mA/°C 2. Derate from 50°C at 0.5mA/°C

Electrical/Optical Characteristics at T_A=25°C

Symbol	Description	HLMP-0904			HLMP-0354			HLMP-0454			HLMP-0554			Units	Test Conditions
		Min.	Typ.	Max.	Min.	Typ.	Max.	Min.	Typ.	Max.	Min.	Typ.	Max.		
I_{VT}	Axial Luminous Intensity	0.5	1.0		1.0	5		1.0	5		0.8	3 At I_F = 25mA		mcd	I_F = 20mA Figs. 3,8,13,16 θ = 0°
$I_{V\theta=}$	Luminous Intensity at θ = 30°[5]	0.3			0.5			0.5			0.4			mcd	I_F = 20 mA θ = 30°
$2\theta_{1/2}$	Included Angle Between Half Luminous Intensity Points		80			70			70			70		deg.	[1] Figures 6, 11, 16, 21
λ_{PEAK}	Peak Wavelength[5]	630	655	700	590	635	686	580	583	660	525	565	600	nm	Measurement at Peak
λ_D	Dominant Wavelength		640			626			585			570		nm	[2]
t_s	Speed of Response		10			200			200			200		ns	
C	Capacitance[5]		200	300		35	100		36	100		36	100	pF	V_F=0; f=1 MHz
θ_{JP}	Thermal Resistance*		425			425			425			425		°C/W	[3]
θ_{JC}	Thermal Resistance**		550			550			550			550		°C/W	[3]
V_F	Forward Voltage		1.8	2.0		2.0	3.0		2.0	3.0		2.1 At I_F = 25mA	3.0	V	I_F = 20mA Figures 2, 7, 12, 17
I_R	Reverse Current[5]			1.0			1.0			1.0			1.0	μA	V_R = 3V
BV_R	Reverse Breakdown Voltage	4	5		5.0			5.0			5.0			V	I_R = 100μA
η_V	Luminous Efficacy		58			140			455			600		lm/W	[4]

NOTES

1. $\theta_{1/2}$ is the off-axis angle at which the luminous intensity is half the axial luminous intensity
2. The dominant wavelength, λ_d, is derived from the CIE chromaticity diagram and represents the single wavelength which defines the color of the device
3. Junction to Cathode Lead with 3.18mm (0.125 inch) of leads exposed between base of flange and heat sink
4. Radiant intensity, I_e, in watts/steradian, may be found from the equation $I_e = I_v/\eta_v$ where I_v is the luminous intensity in candelas and η_v is the luminous efficacy in lumens/watt.
5. Limits do not apply to non JAN parts

*Panel mount

**TO-46

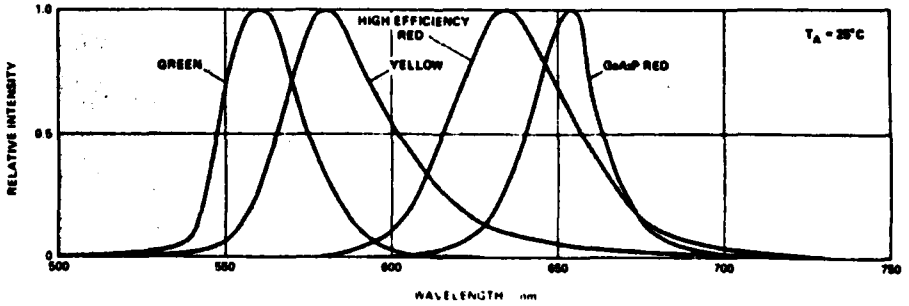

Relative Intensity vs. Wavelength.

D. SIMPLE MODEL OF AN LED

The simplest LED semiconductor model assumes a pn junction created by doping one region with donor atoms and an adjacent region with acceptor atoms. In LEDs, light is produced by energy released in the form of a photon when an electron in the conduction band jumps the gap and recombines with an acceptor in the valence band. The recombination may be direct, where the electron goes across the entire gap in the jump, or indirect where it first recombines at an intermediate energy level and subsequently makes a transition across the remainder of the gap. GaAs and $GaAs_{1-x}P_x$ devices are direct and GaP indirect. The wavelength is given by

$$\lambda = \frac{1240}{\Delta E_g} \quad \text{nm} \tag{2}$$

where ΔE_g is the energy level difference of the direct gap. Table II summarizes common properties for LEDs [Ref. 9]. Gage, et. al., in [Ref. 9] is a good source for further details on LED operation and characteristics.

TABLE II

TYPICAL LED PROPERTIES

Material	Band Energy Gap (eV)	Emission, λ (nm)	Transition Type
GaAs	1.43	910	direct
GaP	2.24	560	indirect
$GaAs_{.60}P_{.40}$	1.91	650	direct

II. BACKGROUND

This chapter includes a survey of radiation sources, a description of the interactions of electrons with matter with respect to radiation damage, some details of LED methods of operation and the effects of electron radiation on LEDs.

A. RADIATION SOURCES

Radiation sources come in a variety of forms. Nuclear weapons output and the Van Allen radiation belts are large scale producers of radiation in several forms. Of course, it is difficult for an investigation of limited means to use these sources directly (and often undesirable as well), so simulators are used to produce scaled down amounts of radiation. The LINAC is such a simulator.

1. Nuclear Weapons

Nuclear weapons upon exploding release several radiation products summarized in Table III [Ref. 10]. Typical output partition for weapon energy is 50-80% into x-ray production, 10-20% into kinetic energy of fission fragments and weapons debris which includes ions and electrons, 1% into neutron production and 0.5% into gamma ray production. About 5% to 10% of the energy may appear as debris decay radiation over extended periods of time, known

TABLE III

SUMMARY OF NUCLEAR WEAPON RADIATION CHARACTERISTICS

Name	Type	Charge	Source	Speed (m/s)	Dispersion
X-ray	Wave	0	Thermal Radiation	3×10^8	Inverse Square Law
γ-ray	wave	0	Nuclear Reaction Fission Fragments	3×10^8	Inverse Square Law
Neutron	particle	0	Nuclear Reaction	$(1.4 \times 10^7)E^{1/2}$	Inverse Square Law
Beta (e^-)	particle	-1	Fission Fragments	3×10^8	Geomagnetic Trapping
EMP Fields	wave	0	Compton Electrons	3×10^8	Inverse First Power Law

as fallout. EMP is electromagnetic pulse, a secondary field effect of the weapon induced Compton electrons. The energy output of a weapon is normally expressed in kilotons (KT) of TNT equivalent where 1 KT = 10^{12} calories.

The number of electrons produced by the weapon directly from debris ionization is significant but not necessarily the major source. For a burst in the atmosphere, the gamma rays induce Compton electrons which are of sufficiently high energy to cause secondary electrons through ionization of the air. The neutrons produced will also cause ionization through collisions with air. This showering effect can produce electron fluxes much larger than the direct weapon production. For instance, if a 1 MeV gamma ray produced one 1 MeV Compton electron, this electron could produce on the order of 30,000 secondary electrons of 33 eV each.

It should be noted that the importance of various weapon outputs to causing electronics upset or degradation does not depend only on the magnitude of the output. Other factors such as the duration time of the pulse are important. Thus gamma rays, though a small percentage of output, can, through their shorter pulse duration, produce a larger amount of electronics upset than the x-rays.

2. Van Allen Belt and Trapped Radiation

Another source for electron radiation is the trapped charged particle regions in the earth's magnetosphere known

as the Van Allen radiation belts. Electrons and protons, as well as larger ions, are trapped in the geomagnetic field by the Lorentz force and spiral around the field lines. The spiraling particles bounce between mirror points that are at conjugate northern and southern hemisphere latitudes. The bounce period is of the order of a tenth of a second. The particles also drift eastward taking about 30 minutes for a 1 MeV electron to drift around the earth [Ref. 10].

Some artificial trapped radiation belts have been created by high altitude nuclear bursts when some of the debris reached sufficient altitudes such that the charged particles were injected into the magnetic field. Some of the artificially produced belts have lasted up to two years with electron fluxes on the order of ten times that of the Van Allen belt. The flux induced by a megaton size device in 1962 produced a peak flux of $\approx 10^9$ electrons/cm^2-sec as measured 10 hours after detonation. Two days after detonation this peak was 5×10^8 electrons/cm^2-sec. The peak Van Allen flux is 1×10^8 electrons/cm^2-sec. Electron energies in the radiation belts go up to 5 MeV. Proton energies reach several hundred MeV [Ref. 10].

3. Linear Accelerator

The various types of radiation encountered in the severe environments outlined above can be simulated using machines and devices of various designs. The production of

electrons for inducing radiation damage was accomplished with the LINAC for this experiment.

The NPS LINAC uses a series of klystrons to impart energy to electrons produced by an electron gun. The beam of electrons is formed and steered by controllable magnets. The beam impacts a target placed in an evacuated target chamber. For this experiment the target chamber was evacuated to 1×10^{-6} Torr with all runs conducted at room temperature ($300^{o}K$).

The peak energy attainable for the electrons is 100 MeV. For this experiment 30-MeV electrons were used. The LINAC operates at 60 pulses per second with a pulse duration on the order of 2.5×10^{-6} sec. The pulses can be single or in pulse trains. There is a theoretical peak of 10^{11} electrons/pulse; however, the accumulated dose or fluence of electrons is spread over an area and actual dose must be measured. The means of doing this was a secondary emission monitor (SEM) directly behind the target. As electrons impacted on the SEM, a capacitor linked to a voltage integrator gave the accumulated dose derived from the relationship

$$q = CV \tag{3}$$

Full operating parameters of the LINAC can be found in [Ref. 12].

B. INTERACTION OF ELECTRONS WITH MATTER

Electrons lose energy in matter by interacting with atomic electrons and nuclei. There are four types of interactions between electrons and matter: elastic collisions with atomic electrons and nuclei and inelastic collisions with atomic electrons and nuclei.

Inelastic collisions are the primary mechanism by which electrons lose energy in matter. Normally, an inelastic collision with an atomic electron results in excitation or freeing of the atomic electron. An inelastic collision with a nucleus deflects the incident electron causing a quantum of electromagnetic radiation (bremsstrahlung) to be emitted. The kinetic energy of the electron is reduced by the amount of energy in the photon produced.

In elastic collisions the incident electron is deflected but does not radiate energy. The electron loses only enough energy to conserve momentum when it collides with a nucleus. For an elastic collision with an atomic electron, energy and momentum are conserved and not enough energy is transferred to ionize the atom. In either case, the effects of elastic collisions are not signficant when considering displacement defects and these types of collisions are ignored.

An electron will undergo all four types of interactions while being stopped by matter. Which interaction occurs is a matter of chance and the probability of each type of

encounter can be obtained from scattering theory. The most probable collision energy loss per mass thickness is for inelastic collisions with atomic electrons and is called collision stopping power. Collision stopping power is directly proportional to the atomic electron density of the struck atom. Thus higher atomic number elements have a greater chance of interaction with an incident electron. Collision stopping power is inversely proportional to the square of the incident electron velocity. Thus a higher energy electron with a higher velocity has a lower chance of interacting in a given thickness with a given material.

Collision stopping power is expressed as a cross section represented by σ_c (sigma) and given in units of MeV-cm^2/gm. Tabulated values for collision stopping powers for selected elements against electrons of selected energies are available. The value used in this experiment was

$$\sigma_c = 1.573 \ \frac{\text{MeV cm}^2}{\text{gm}} \qquad (4)$$

from the table for copper and 30-MeV electrons [Ref. 13]. Copper was used as this is the closest atomic number element to Gallium and Arsenic for which tabulated figures were available.

There is a second consideration for the stopping of the electron because of its loss of energy to radiation

(bremsstrahlung) during inelastic collisions with atomic nuclei. This effect is contained in a second cross section, σ_R, and the total stopping power of a material is the sum of the collision and radiative stopping powers. Radiative stopping power was ignored for this experiment because the damage of interest is displacement defects in the material structure and these permanent defects are predominantly a result of the collisions with the atomic electrons. It should be noted that the bremsstrahlung, which extends in frequency up to γ (gamma) radiation, can contribute to electron production and be a multiplying factor for total dose sustained by a material. These γ-rays have high penetrating power and the secondary electron production is more of a volume effect. The small size of the LEDs in this experiment allowed this effect to be ignored.

In this report electron dose is expressed in several ways. The simplest is fluence, given by total electrons/cm^2. It is also expressed by flux in terms of electrons/cm^2-sec. Finally the dose may be given in rads. This is an expression of the total amount of energy transferred to the material by the radiation. One rad is the same as 100 ergs/gm. Rads must be specified for the material such as "rads (Cu)" for copper because the amount of energy transferred is dependent on the collision stopping power cross section, a function of the material. Dose given

in rads will always be in rads (Cu) for this report unless otherwise specified.

Since in an LED the volume where light production occurs is such a thin section, the concept of surface dose is used. Surface dose is dose deposited on a surface rather than in a volume. According to Rudie [Ref. 10], the surface dose in rads for a low atomic number material irradiated by Φ (phi) monoenergetic electrons per square centimeter can be expressed by

$$R \text{ (rads)} = 1.6 \times 10^{-8} \Phi \sigma_c \qquad (5)$$

where σ_c is given by equation 4 for copper and the conversion factor 1.6×10^{-8} is for converting MeV to units of 100 ergs. This formula will be used for doses given in rads in this report.

C. EFFECTS OF ELECTRON RADIATION ON LEDs

LEDs are a well investigated and well understood class of semiconductor devices. The operation of the LEDs will not be covered in detail except that the basis for current flow in the devices will be explained. Using the simplest current relationships the damage constant, a useful parameter for phenomenological description of radiation damage effects, is derived. Two excellent sources for further details on LED theory, as well as other semiconductors, are

found in Muller and Kamins' Device Electronics for Integrated Circuits [Ref.14] and Sze's Physics of Semiconductor Devices [Ref. 15].

1. LED Current

In Muller and Kamins [Ref. 14], Chapter 4, an analysis of currents in a pn junction of an ideal diode is done.

The first step is to obtain a continuity equation across the infinitesimal slice, dx, representing the pn junction. This continuity equation for free carriers accounts for the net flow of electrons (or positive charge carriers called holes) into and out of the slice and the excess generation over recombination of electrons within the slice. This leads to complicated partial differential equations. They are simplified using assumptions about the nondependence on x of diffusion and about mobility parameters for the carriers. Steady state is assumed and the equations become ordinary differential equations in x. The electric field is assumed to be negligible in the region under consideration and the equations become

$$D_n \frac{d^2 n(x)}{dx^2} = R_n - G_n \qquad (6)$$

and

$$D_p \frac{d^2p(x)}{dx^2} = R_p - G_p \qquad (7)$$

where D_n and D_p are the diffusion constants for the electrons and holes respectively (not functions of x), n(x) and p(x) are the number concentrations of electrons and holes respectively and R_n, R_p, G_n and G_p represent the recombination and generation rates of the carriers.

Generation and recombination models developed by Shockley, Hall and Read (SHR) are applied to the resulting equations. It is then possible to characterize the minority carrier distributions in the pn junction under bias. A solution for an ideal diode can then be obtained.

The ideal diode model, using the SHR model, uses a pn junction connected to a voltage source with the negatively doped n region grounded and the positively doped p region at V_a volts (Figure 2) relative to ground. It is assumed that the applied voltage V_a is sustained entirely at the junction. If V_a is positive, for forward bias, the barrier to the diffusion flow of majority carriers at the junction is reduced. The reduced barrier permits a net transfer rate of holes from the p-side to the n-side and of electrons from the n-side to the p-side. The transferred carriers become minority carriers and are quickly neutralized. Minority carrier densities and lifetime are a

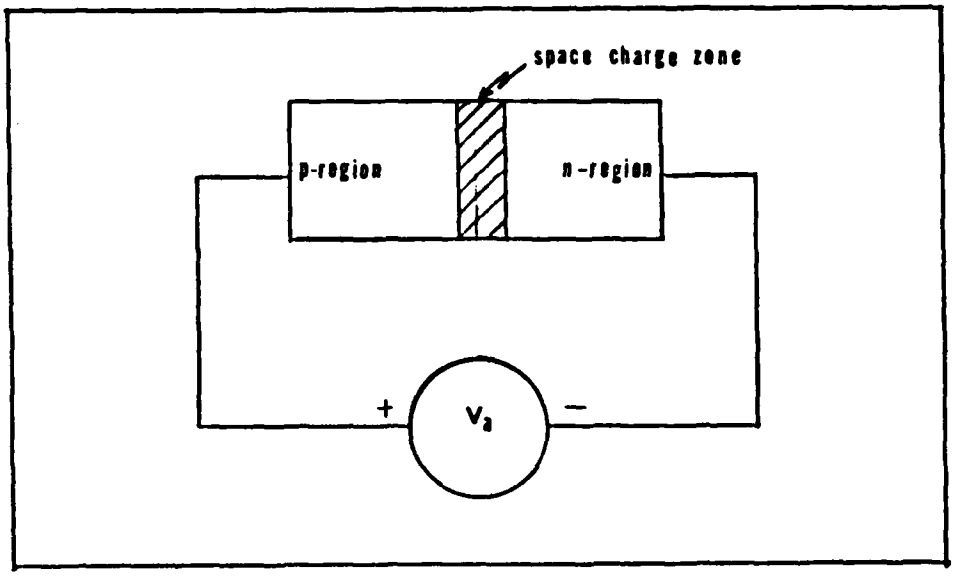

Figure 2. Simple pn Junction Diode

critical parameter because they determine what currents flow in a pn junction. Majority carriers act as suppliers of the injected minority-carrier current or as charge neutralizers. The final relation for current as a function of applied voltage V_a is

$$J = J_o \left[\exp(qV_a/kT) - 1\right] \tag{8}$$

where J is total current, the sum of diffusion current and drift current, and J_o is the saturation current arrived at by negative biasing the diode to the breakdown point.

As explained above, minority carrier concentration and lifetime are the important parameters for determining

diode operation. Minority carrier concentrations are typically 10 orders of magnitude below majority carrier densities [Ref. 14]. The carrier densities and thus the current are dependent on the applied voltage according to the equation

$$pn = n_i^2 \exp(qV_a/kT) \tag{9}$$

and

$$J = J_o \exp(qV_a/kT) \tag{10}$$

becomes the working equation under forward bias. The component due to saturation current is ignored as is the drift current since they are much smaller in normal operation than the total forward current. In these equations, J is total current, n_i is the intrinsic carrier concentration, q is the unit of charge, k is the Boltzmann constant, and T is temperature in ^{o}K.

This simple model of the pn junction (Figure 2) treated the junction simply as a barrier to the diffusion of carriers. Under certain conditions the junction, which has dimensions on the order of 10^{-4} cm, can act as a depletion region. A significant number of recombinations can take place in this so-called space charge recombination region. Using assumptions similar to those above, the carrier densities for this space charge recombination region are found to be

$$p = n = n_i \exp(qV_a/2kT) \quad (11)$$

and the current relation is

$$J = J_o \exp(qV_a/2kT) \quad (12)$$

The total current for a pn junction is a combination of the diffusion current and space charge recombination current although one or the other is often dominant. The dominant current type can be determined by examining a voltage versus current plot for the LED as in Figure 7. By measuring the slope of the straight part of the curve a value for the constant in the denominator of the exponential (1 for Eqn. 10 or 2 for Eqn. 12) can be obtained. If it is close to 1, diffusion current is dominant and, if it is close to 2, space charge recombination current is dominant.

2. Damage Effects and Determination

The light output of the LED is related to the efficiency of conversion of forward biased current. Degradation of the light output is caused by the introduction of nonradiative recombination centers into the semiconductor structure. These centers compete with radiative centers for excess minority carriers. The result is a reduction in minority carrier lifetime τ.

B.H. Rose and C.E. Barnes in [Ref. 8] outlined a derivation for determining a damage parameter as follows.

Total initial lifetime of the minority carriers is written

$$\frac{1}{\tau_0} = \frac{1}{\tau_{OR}} + \frac{1}{\tau_{ONR}} \tag{13}$$

where τ_0 is the preirradiation minority carrier lifetime and τ_{OR} and τ_{ONR} are the lifetimes associated with radiative and nonradiative processes. The lifetime values are determined by the equations

$$\frac{1}{\tau_{OR}} = \sigma_R \, v_{th} \, N_R \tag{14}$$

and

$$\frac{1}{\tau_{ONR}} = \sigma_{NR} \, v_{th} \, N_{NR} \tag{15}$$

where σ_R and σ_{NR} are carrier capture cross sections and v_{th} is the minority carrier thermal velocity. N_R and N_{NR} are the radiative and nonradiative center concentrations, respectively.

The minority carrier lifetime after irradiation is expressed in a phenomenological equation as

$$\frac{1}{\tau} = \frac{1}{\tau_{OR}} + \frac{1}{\tau_{ONR}} + \sigma_{NRI} \, v_{th} \, N_{NRI} \tag{16}$$

where the additional term comes from the radiation introduced nonradiative centers. This can be rewritten as

$$\frac{1}{\tau} = \frac{1}{\tau_0} + \sigma_{NRI}\, v_{th}\, N_{NRI} \tag{17}$$

and

$$N_{NRI} \equiv C_1\, \Phi \tag{18}$$

where Φ is the radiation fluence in electrons/cm^2 and C_1 is a constant reflecting the probability of generation of a defect by a unit of fluence.

The physics governing the effects of radiation on the semiconductor material is contained in the damage constant K,

$$K \equiv \sigma_{NRI}\, v_{th}\, C_1 \tag{19}$$

and the equation used to describe LED radiation damage is

$$\frac{1}{\tau} = \frac{1}{\tau_0} + K\, \Phi \tag{20}$$

or

$$\frac{\tau_0}{\tau} = 1 + \tau_0\, K\, \Phi \tag{21}$$

Determining or predicting LED light output degradation by the phenomenological approach is useful. $\tau_0 K$, the initial lifetime-damage constant product is the quantity of interest.

The current controlling mechanism for the operating region of the device must be known to determine the damage constant. For an LED whose light output is due to a diffusion controlled radiative current the light output would be given by [Ref. 8]

$$I = C_2 \tau \exp(qV_a/kT) \tag{22}$$

where C_2 incorporates the LED conversion efficiency. Taking the ratio of I_0 and I (where I_0 and I are the pre- and post-radiation light outputs and τ_0 is the value in Eqn. 22 for I_0) gives the first half of Eqn. 23. The rest follows from Eqn. 21.

$$\frac{I_0}{I} = \frac{\tau_0}{\tau} = 1 + \tau_0 K \Phi \tag{23}$$

By measuring I_0 and I as a function of Φ the value of $\tau_0 K$ is determined.

According to Sze [Ref. 15], total current density, J, when dominated by diffusion is expressed as

$$J = \frac{C_3}{\tau^{1/2}} \exp(qV_a/kT) \quad (24)$$

where C_3 is a constant similar to C_2. Solving for $\exp(qV_a/kT)$ and substituting into Eqn. 22 gives

$$I = C_4 \tau^{3/2} J \quad (25)$$

where C_4 is the product of the constants C_2 and C_3. It can be seen from Eqn. 25 that in this case τ is proportional to $I^{2/3}$ for constant total current J. Substituting from Eqn. 21 then gives

$$\left(\frac{I_0}{I}\right)^{2/3} = \left(\frac{\tau_0}{\tau}\right) = 1 + \tau_0 K \Phi \quad (26)$$

The difference between Eqn. 26 and Eqn. 23 is the condition of constant total current J which is a condition that can be maintained experimentally.

If the device total current (J) is dominated by space charge recombination the current is found, according to Sze [Ref. 15], as

$$J = \frac{C_5}{\tau} \exp(qV_a/2kT) \quad (27)$$

and following steps similar to above with radiative current (I) diffusion controlled, the equation of interest becomes

$$\left(\frac{I_0}{I} \right)^{1/3} = \frac{\tau_0}{\tau} = 1 + \tau_0 K \Phi \qquad (28)$$

Finally if the radiative current (I) is space charge recombination controlled and the total current (J) is space charge recombination controlled, according to Rose and Barnes [Ref. 8] the equation is

$$\frac{J}{J_0} = \frac{\tau_0}{\tau} = 1 + \tau_0 K \Phi \qquad (29)$$

Table IV summarizes the light output degradation equations discussed. In the table I and I_0 are the radiative currents and J_0 and J are the total currents, radiative plus nonradiative. In the derivations the values for total currents are actually current density and the values for radiative current should be likewise. In this experiment the currents are measured, rather than current densities. For the radiative currents, relative intensities are measured. Since the currents are used in ratios it is possible to use the values as measured this way. This assumes that the device area stays constant.

TABLE IV

EQUATIONS FOR ANALYSIS OF LIGHT OUTPUT DEGRADATION IN ELECTRON IRRADIATED LEDs

1)	$\left[\left(\frac{I_0}{I}\right)^{2/3} - 1\right] = \tau_0 K \Phi$	I: Diffusion J: Diffusion
2)	$\left[\left(\frac{I_0}{I}\right)^{1/3} - 1\right] = \tau_0 K \Phi$	I: Diffusion J: Space Charge
3)	$\left[\left(\frac{J}{J_0}\right) - 1\right] = \tau_0 K \Phi$	I: Space Charge J: Space Charge

III. EXPERIMENTAL PROCEDURES

The LEDs in this experiment were characterized before and after irradiation. Details of the measurements are given in this chapter along with some comments on the LINAC and its operation. Experimental results are given in Chapter IV.

A. LIGHT EMITTING DIODES

The physical configuration of the LEDs provided by Hewlett Packard has already been described. It should be reemphasized that all measurements and irradiation runs were done with the plastic cap and glass lens of the LEDs removed and the LEDs as discrete devices.

Four LEDs, one for each color, were measured for relative intensity versus wavelength using a modified Beckman DK-1A photospectrometer and strip chart recorder. They were all measured at a set current and forward bias level. They were then irradiated to a level of 7×10^{12} electrons/cm^2 (e^-/cm^2) and measured again on the Beckman DK-1A.

Samples of the lens and red and green plastic cap material were irradiated to levels of 7×10^{13} e^-/cm^2 and 2×10^{14} e^-/cm^2. Measurements for transmission of visible and infra-red spectrum light were made on the samples before

and after irradiation. The instruments used were a Perkin-Elmer (PE) 330 photospectrometer for the range 185 nm up to 2500 nm, a PE 137G for the range 2500 nm to 7500 nm and a PE 387 for 7500 nm to 25000 nm.

Twelve LEDs, one of each color in three groups, were characterized for total absolute output intensity in microwatts using a Fiber Optics 550 power meter with a model #255 detector. The LEDs were connected in series with a precision 120Ω current setting resistor and a Hewlett-Packard 6216A power supply. The power supply was set to values of 4.0 volts and 6.0 volts for two series of measurements. Fluke 75 multimeters were used to measure circuit current and voltage dropped across the LED (V_a). The meters were accurate to $\pm$0.01 mA and $\pm$0.01 V. A series of measurements was conducted on the power meter by varying the current at the power supply. Thus a series of voltage versus current versus output intensity readings were obtained. Each LED was characterized twice, once with the power supply at 4.0 volts and once with the power supply at 6.0 volts, which gave higher current values.

The Fiber Optics 550 power meter measures the output intensity of the LED and compares it to a calibrated microwatt internal reference. A correction factor based on the dominant wavelength of the LED is applied to a decibel reading and a value for intensity in microwatts can be determined according to

$$(\text{reading} + \text{correction})\ dB\mu = 10\ LOG_{10}\ \frac{I}{\mu W} \qquad (30)$$

or

$$I = 10^{(\text{reading} + \text{correction})/10}(\mu W) \qquad (31)$$

After this initial characterization the LEDs were mounted on a rack in groups of four at a time, one of each color. This rack was mounted in the LINAC target chamber. The rack could be moved up and down and rotated so that each LED could, in turn, be put in the path of the electron beam. A switchable circuit was set up so that each LED could be powered separately. The power supply and voltage/current measuring meters were the same as for the preliminary characterizations.

Each LED was characterized while in the evacuated target chamber. The voltage/current values were varied at the LINAC control station using the same values as the preliminary characterizations. The LED light output intensities were measured for relative output using a simple photodetector cell placed in the target chamber out of line of the electron beam as in Figure 3. The values for intensity were recorded from a digital conversion meter and as the ordinate on an analog X-Y recorder. Each LED was irradiated in four separate steps. During irradiation the X-Y recorder plotted the light output of the LED being

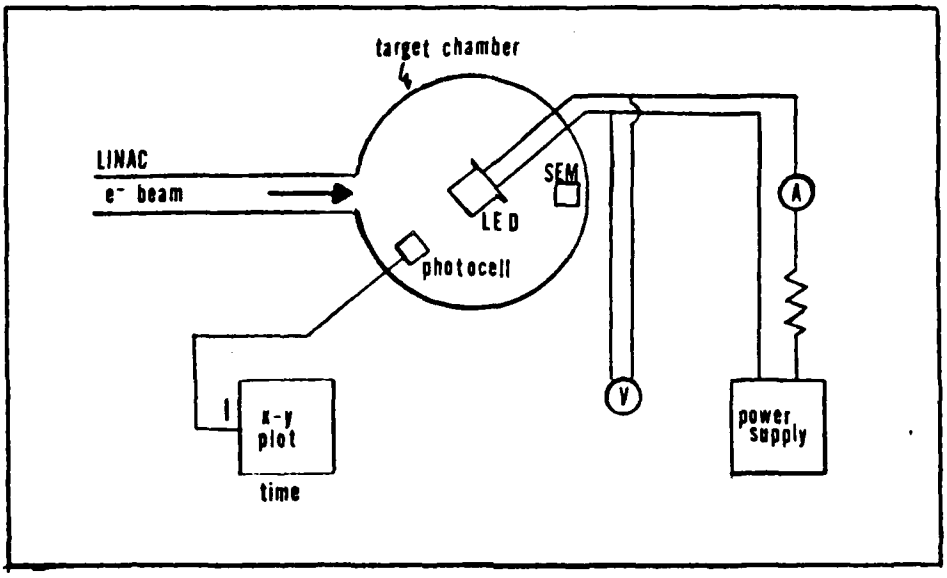

Figure 3. LINAC Irradiation Configuration

irradiated versus time on the abscissa. The LED was powered at 4.0 volts or 6.0 volts with current set by the 120Ω resistor. After each step of irradiation the X-Y recorder continued to plot intensity versus time for about five minutes. After each run the LED was characterized for voltage versus current as in the preliminary characterization. Two groups of LEDs were irradiated using the 4.0 volt power setting and one group using the 6.0 volt setting.

Thirty days after irradiation the LEDs were characterized using the Fiber Optics 550. The time delay was to allow any annealing that might occur to take place.

B. LINEAR ACCELERATOR

As noted earlier, the number of electrons received at the target was measured by an SEM using a capacitor connected to a voltage integrator to determine the charge. The SEM is accurate to $\pm$5%.

The electron beam size was focused to an area of .7 cm^2. This was measured by examining the darkening pattern on the plastic LED cap material for several samples. However, for each run the beam had to be refocused. A television camera was positioned to observe the target area. A piece of phosphor screen was mounted on top of the rack and an outline of the preset beam size drawn on the television monitor. This rather crude method of focusing gives an estimated error to the beam intensity of $\pm$20%.

The SEM was 6% efficient and the capacitor had a value of .05 microfarads. Thus, on a per volt basis, the reading from the integrator gives the number of electrons/cm^2 computed as follows:

$$q = CV \tag{32}$$

but per volt

$$C = .05 \times 10^{-6} \text{ F/V} \tag{33}$$

and

$$q = 5 \times 10^{-9} \text{ coulomb/V} \tag{34}$$

and there are

$$6.24 \times 10^{18} \text{ electrons/coulomb} \quad (35)$$

so the number of electrons is

$$\#\text{ electrons} = (6.24 \times 10^{18})(5 \times 10^{-8}) = 3.1 \times 10^{11}/V \quad (36)$$

However, the SEM is only 6% efficient and the beam size is .7 cm^2 so

$$\#\text{ electrons/cm}^2 = \frac{3.1 \times 10^{11}}{(.06)(.7)} = 7 \times 10^{12}/V \quad (37)$$

This value can be expressed as rads (Cu) by Eqn. 5

$$R = (1.6 \times 10^{-8})(7 \times 10^{12})(1.573) = 2 \times 10^{5} \text{ rads (Cu)}/V \quad (38)$$

The four irradiations of each LED were in steps of 0.1 volts, 0.5 volts, 2.4 volts, and 3.0 volts each. This gave cumulative totals after each run of 0.1 volts, 0.6 volts, 3.0 volts, and 6.0 volts. This is summarized in Table V.

The values for fluence and dose are rounded because of the inaccuracy in the measurement of the electron beam. Additional error is introduced because the beam was manually controlled and the exact turn off point on the voltage integrator was determined by operator eye-hand coordination. Additionally, the beam could easily detune itself during a

TABLE V

CUMULATIVE IRRADIATION LEVELS FOR LINAC RUNS

Voltage (Integrator)	Fluence (e/cm^2)	Dose (rads)
0.1	7×10^{11}	1×10^{4}
0.6	4×10^{12}	1×10^{5}
3.0	2×10^{13}	5×10^{5}
6.0	4×10^{13}	1×10^{6}

run. The operator could detect this by seeing a change in the progress rate of the analog voltage integrator meter and could correct it. It is possible that the actual dose sustained by an LED is only accurate to $\pm$25%. The rate at which the dose was received could vary by an even larger amount.

Another problem in determining dose is the distribution of the beam. The actual distribution of the beam is not known but presumed to be roughly Gaussian. Thus the electron fluence received by a target in the center of the beam could be significantly higher than on the perimeter of the beam. In this experiment the relative alignment of the rack to the beam was constant and it is felt that this distribution problem was corrected for as much as possible. The fluences and doses for the whole beam are still accurate as detailed above, but the dose received at one point in the LED could be higher by a factor of up to two.

Another factor affecting dosimetry would be secondary production of electrons from the bremsstrahlung gammas. As explained before, these gammas were ignored due to their penetrating power but some contribution to dosage can be presumed.

C. TEMPERATURE CONSIDERATIONS

Throughout the measurements constant temperature ($300^{\circ}K$) is presumed. Due to the transfer of energy to the devices and the absence of an atmosphere to conduct away heat in the target chamber it is possible that a significant temperature rise could occur. The thermal radiation dose is

$$D = \Delta T \, C_p \, \rho M \tag{39}$$

where D is the dose in calories and C_p is the specific heat of the material ($cal/^{\circ}K$-mole) and ρ is the density and M the mass of the material. The estimated maximum temperature rise for the maximum dose applied in the longest irradiations was $20^{\circ}K$. This is not sufficient to cause damage to the LED. The V-I characteristics of the LEDs will be altered slightly.

IV. RESULTS AND DISCUSSION

This chapter presents the results of irradiation of LEDs with 30-MeV electrons. First an array of graphs is presented which tabulates the data taken in a readable form. The effect of radiation damage on total current and radiative current is then shown along with the effects on the plastic cap and glass lens materials. The effect on radiative current is presented in terms of intensity versus time and then intensity versus dose. These two presentations show intensity in normalized or arbitrary units for each cumulative dose applied to the LED. Also given in Appendix A are tables of absolute intensity versus forward bias and current. Discussions of results are included with the explanations of the presentations. Conclusions and ideas for further work are given in Chapter V.

A. PLASTIC CAP AND GLASS LENS

The plastic cap material and glass lens samples were irradiated separately. Since the intensity of an LED was to be measured in the target chamber, any darkening that might occur in these two components would have interferred with measurements. The damage sustained by these components, affecting output intensity, would be added onto the damage sustained by the LED itself. The dosages applied to the

lens and cap materials were an order of magnitude greater than the maximum dosage applied to any LED.

Both types of materials were measured on the Perkin-Elmer photospectrometers where transparency versus wavelength was recorded (Figures 4 and 5). The devices use a radiant source and measure the amount of intensity transmitted, compared to a reference sample. Figures 4 and 5 show the results in the visible light range. Measurements were also done in the infrared region but showed no significant change after irradiation. In the visible region, there is a 30% reduction of transparency at 550 nm for the plastic cap material and a 15% reduction of transparency for the glass lens material. An interesting phenomenon (not investigated further) was that the darkened portion of the plastic material lightened almost to its original color when measured first on the infrared machine. This was possibly due to warming of the plastic from the infrared source.

The lenses were found to be orientation sensitive. An effort was made to always have the lens in the same position when working with it. It was not determined whether this effect was due to polarization or simply imperfection in the lens shape or mounting.

B. LED WAVELENGTH ALTERATION

Several preliminary runs were conducted on LEDs with dosages of up to 1 MRad. The LEDs were measured before and

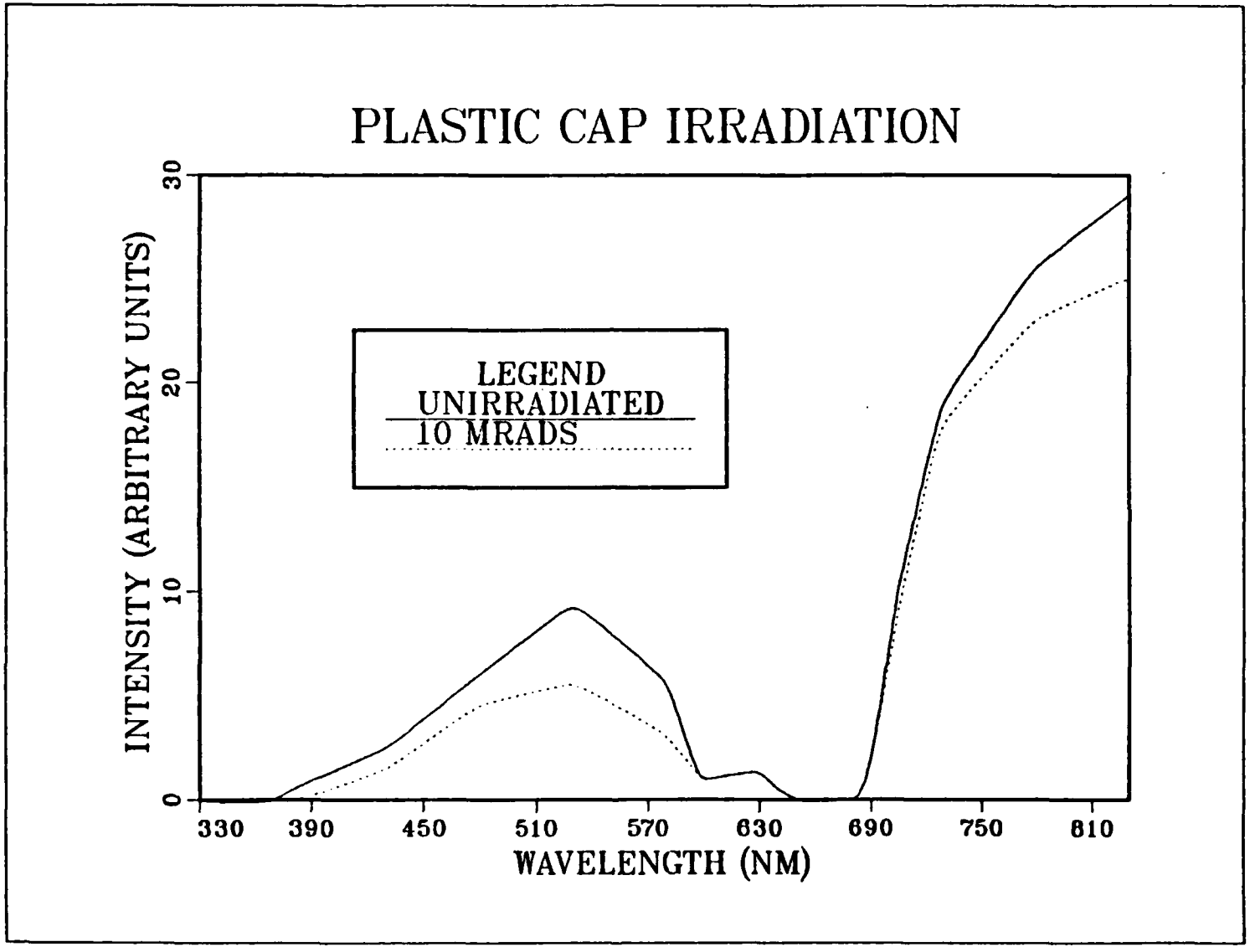

Figure 4. Plastic Cap Material Irradiation Effects

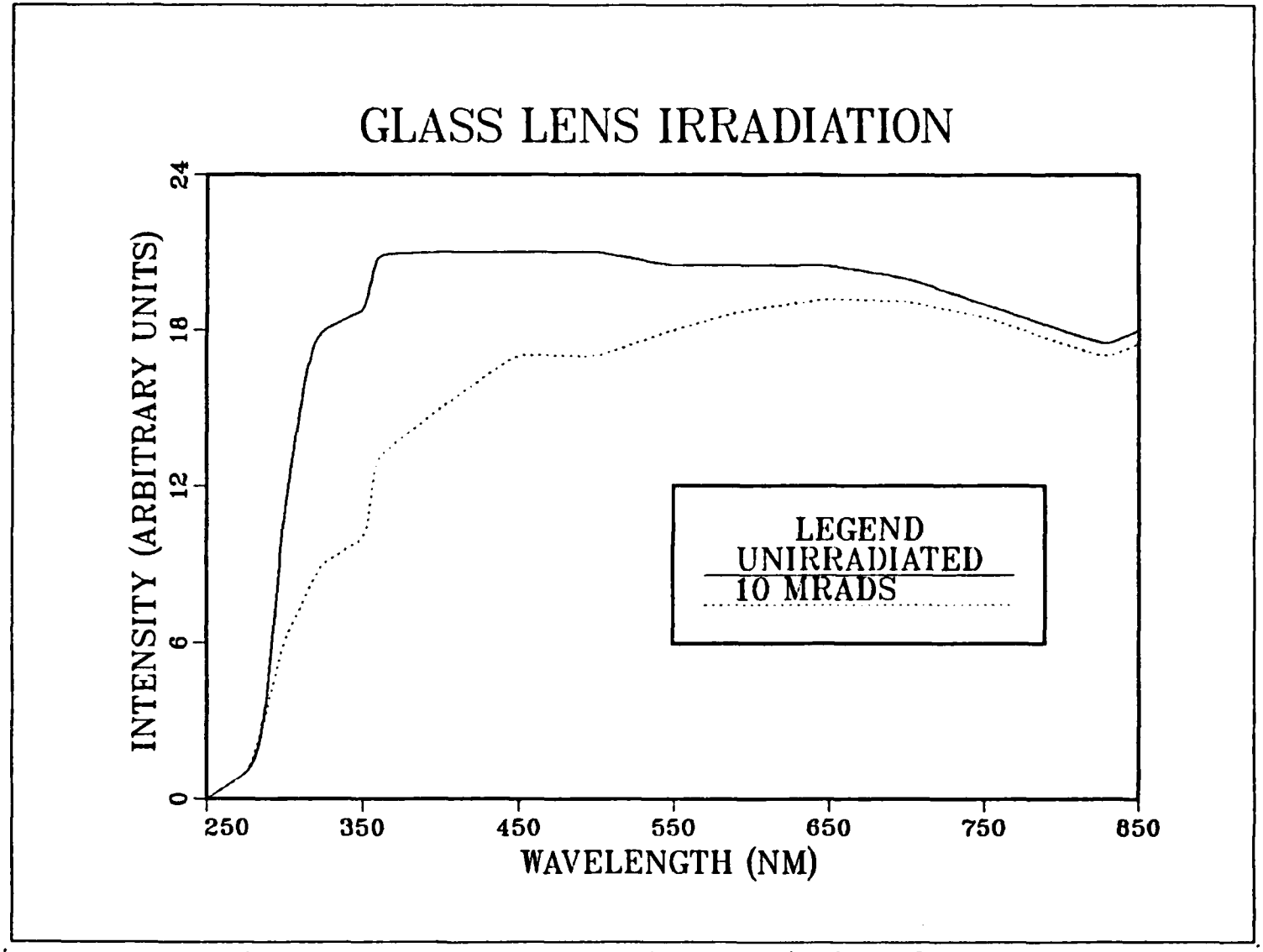

Figure 5. Glass Lens Material Irradiation Effects

after irradiation for relative output versus wavelength using the modified Beckman DK-1A photospectrometer. The LED replaced the light source and a prism dispersed this light by wavelength which was then collected by the machine's photomultiplier tube. The purpose was to see if any shift in wavelength occurred due to radiation damage and to determine dose levels to use in later runs. A typical example of the result after 180 KRads (Cu) is shown in Figure 6. The intensity was reduced significantly but there was no detectable shift in wavelength.

C. LED CURRENT VERSUS FORWARD BIAS

Figures 7 through 14 show the voltage versus current (VI) characteristics curves for the LEDs tested. There are two graphs for each color of LED, one with a single LED powered by 6.0 volts at the power supply, labeled "high current mode", and one with two LEDs powered by 4.0 volts at the power supply. On each graph, each LED has five curves associated with it. One curve represents the characteristics before irradiation and four curves show the characteristics after each level of irradiation. The doses are cumulative and the curves represent the values for the cumulative levels.

On the graphs each curve is indicated by a distinctive mark for each level of irradiation. Additionally, under each curve labeled in the legend is a solid line or dashed

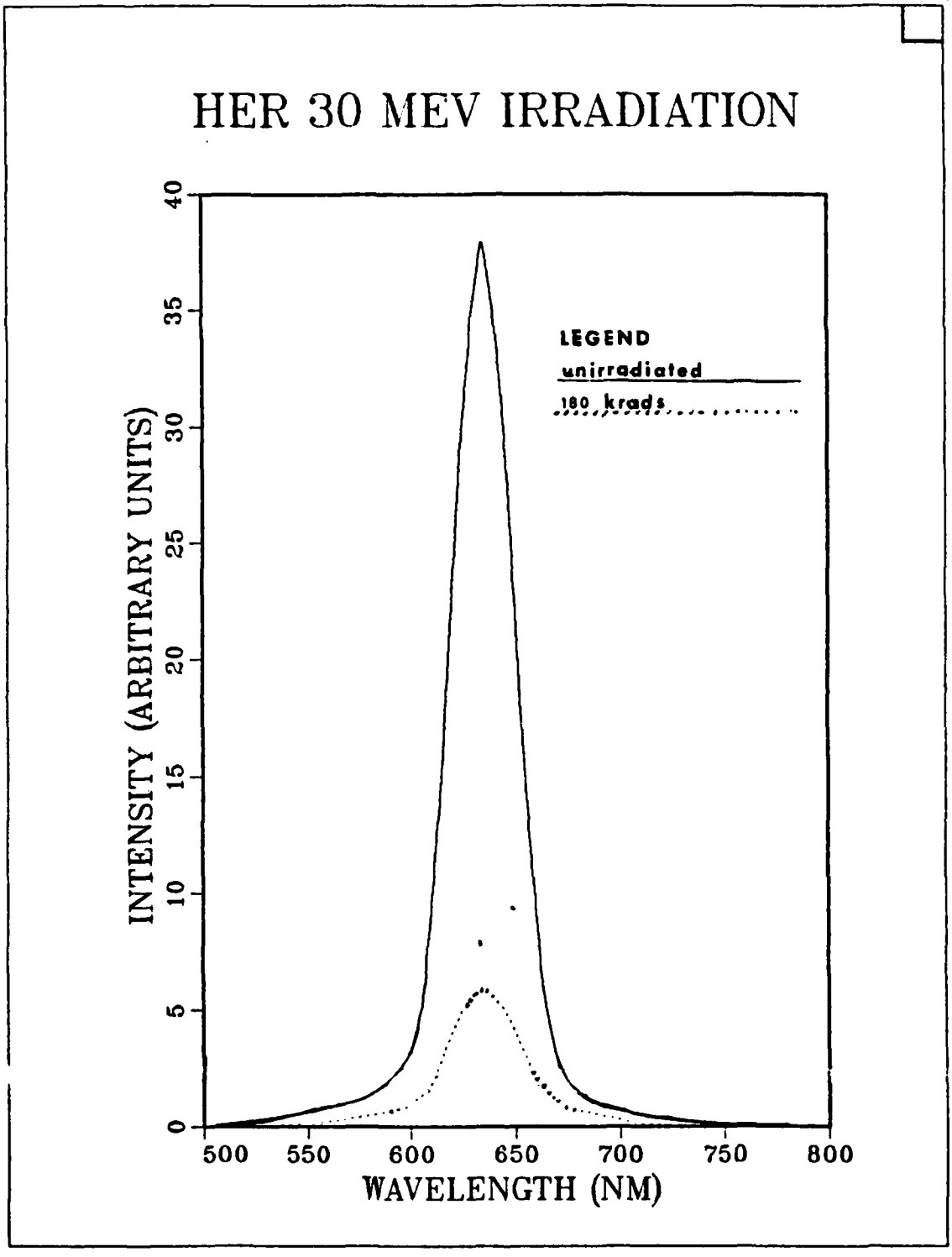

Figure 6. LED Intensity versus Wavelength

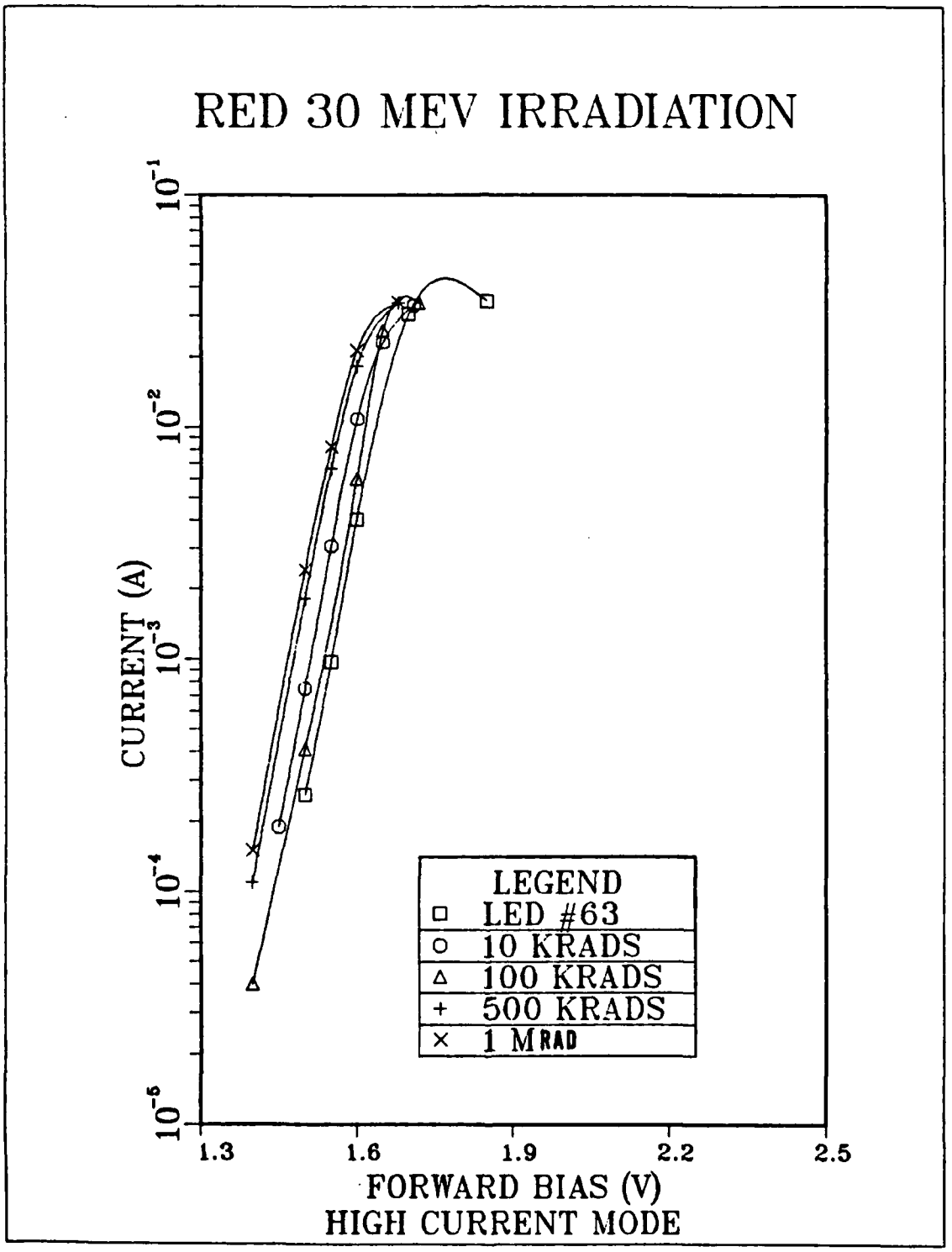

Figure 7. VI Characteristics for Red LED in High Current Mode

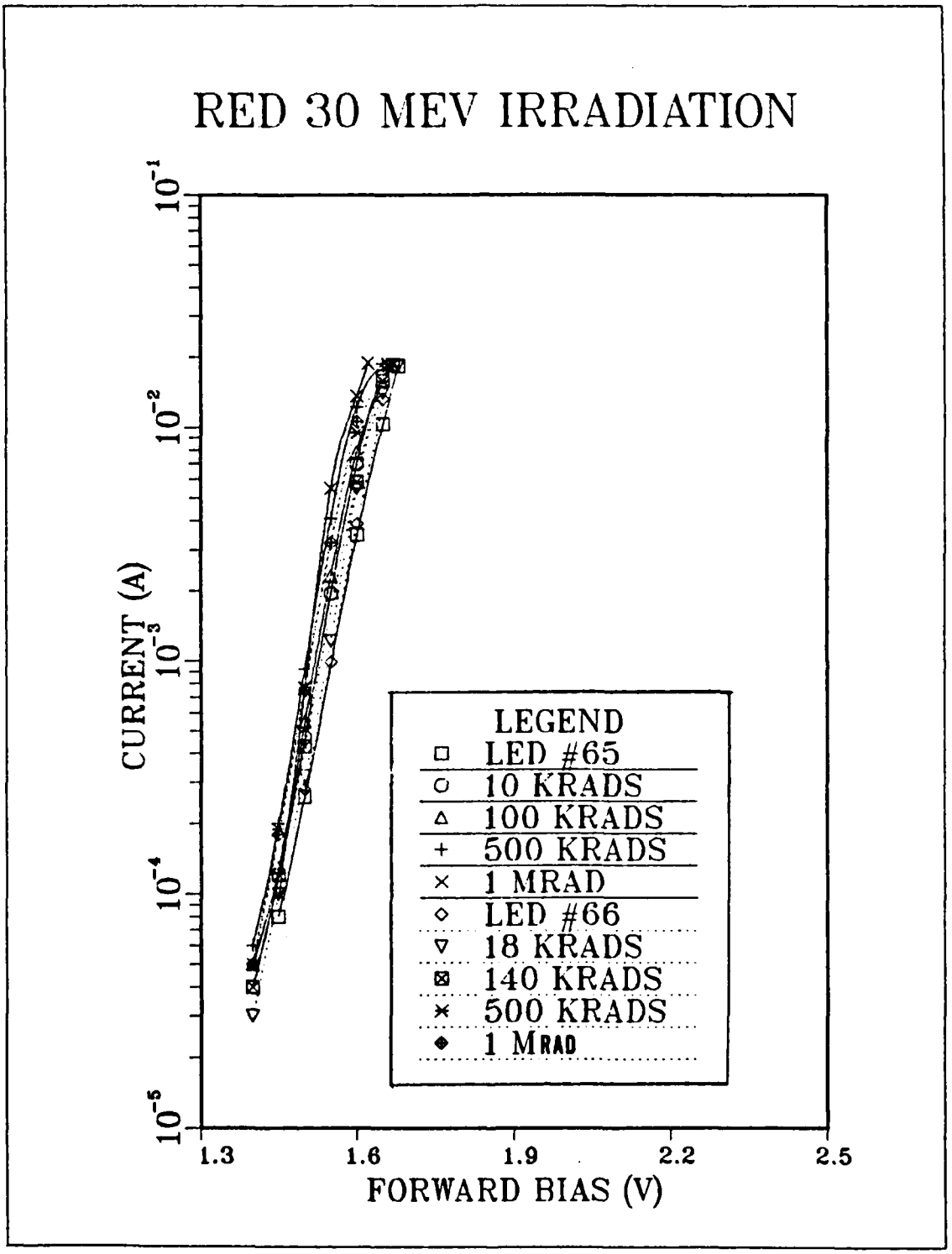

Figure 8. VI Characteristics for Red LEDs in Low Current Mode

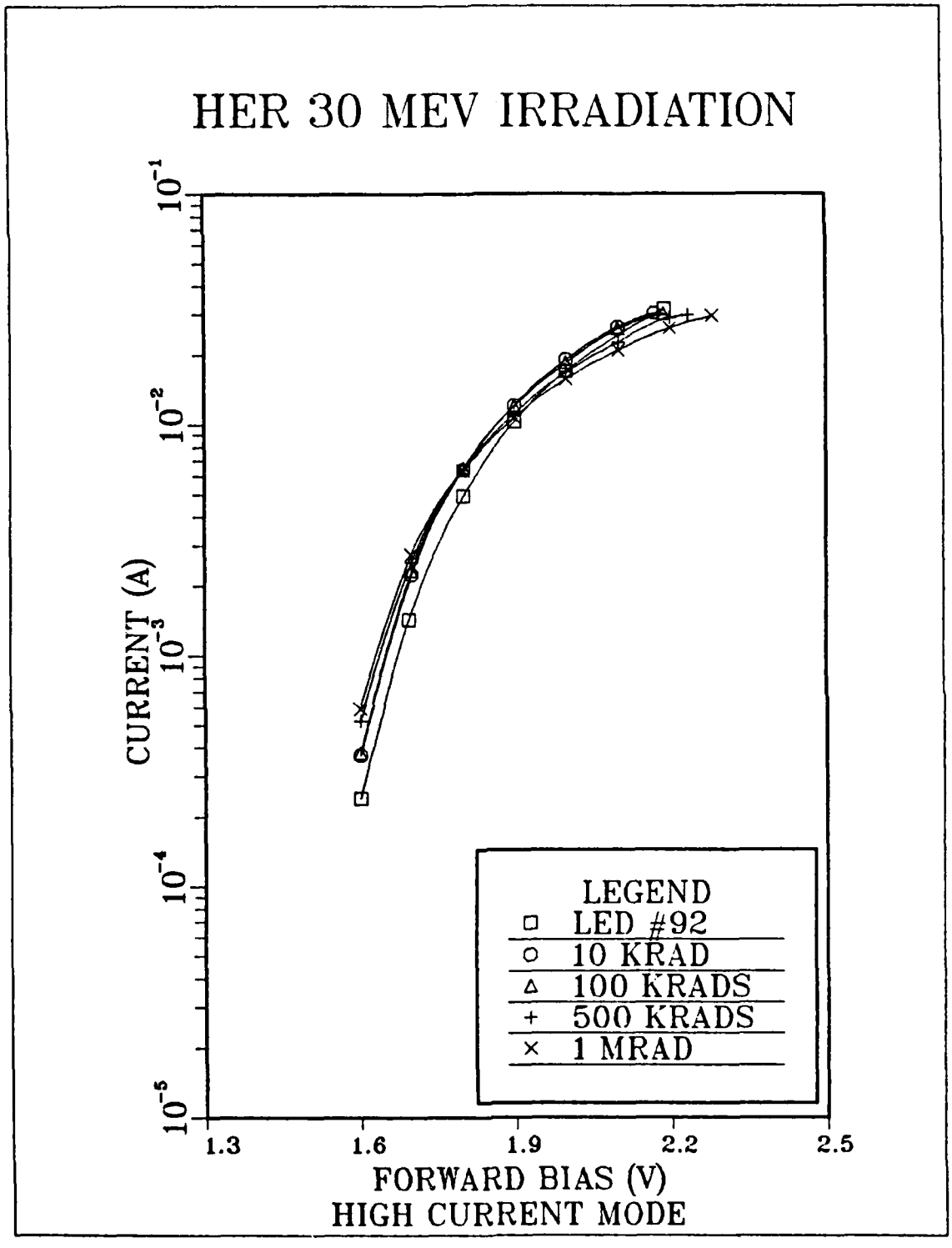

Figure 9. VI Characteristics for High Efficiency Red LED in High Current Mode

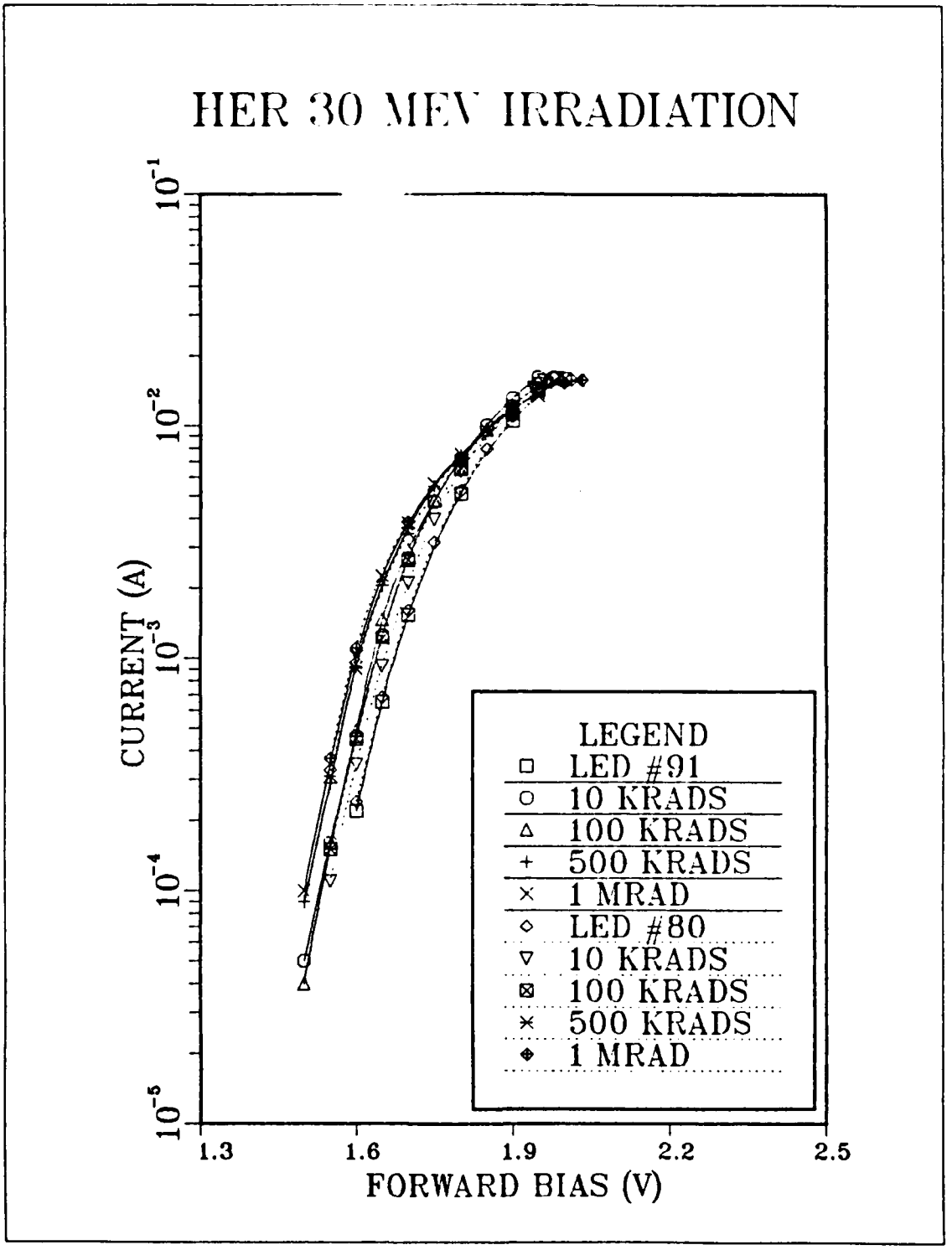

Figure 10. VI Characteristics for High Efficiency Red LEDs in Low Current Mode

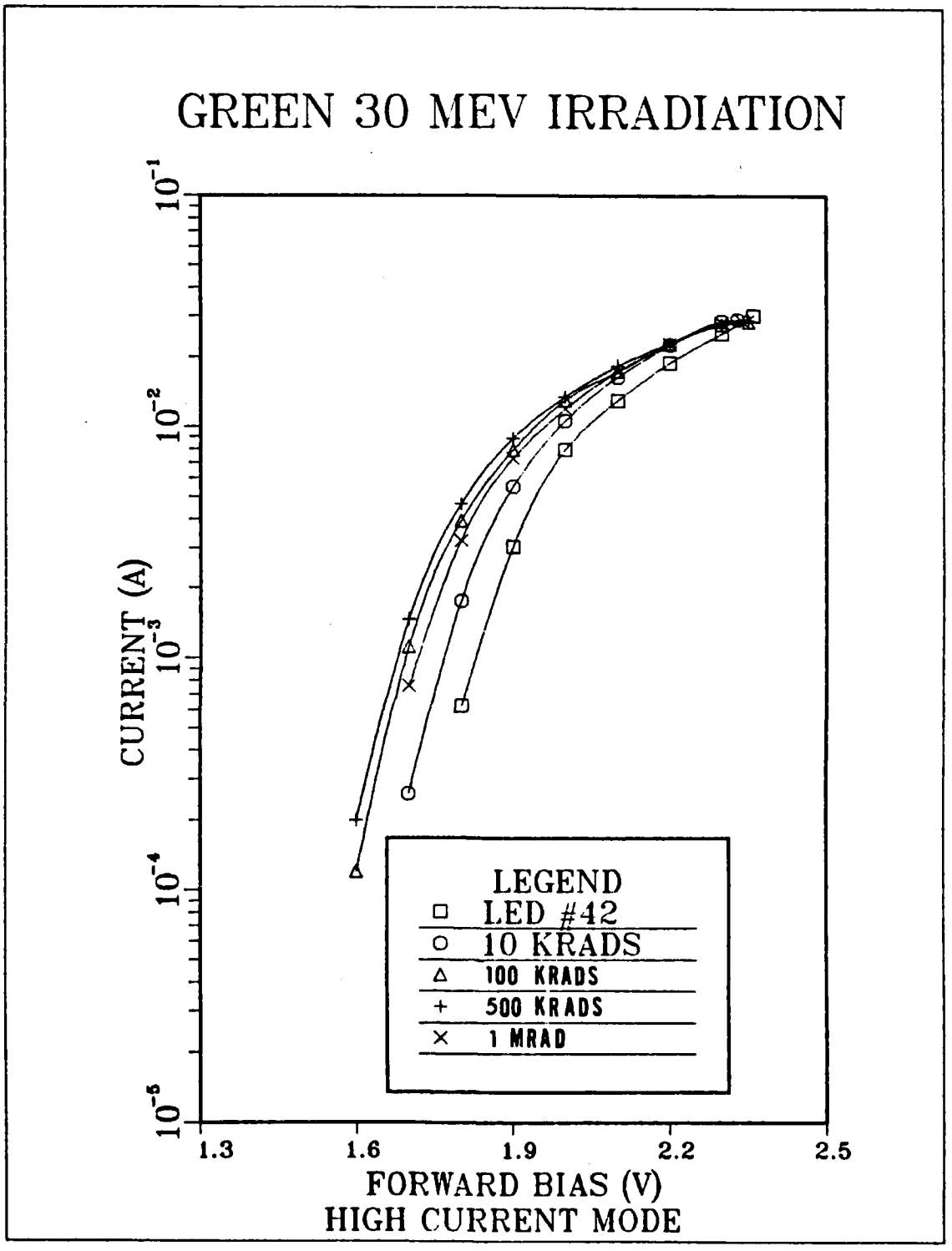

Figure 11. VI Characteristics for Green LED in High Current Mode

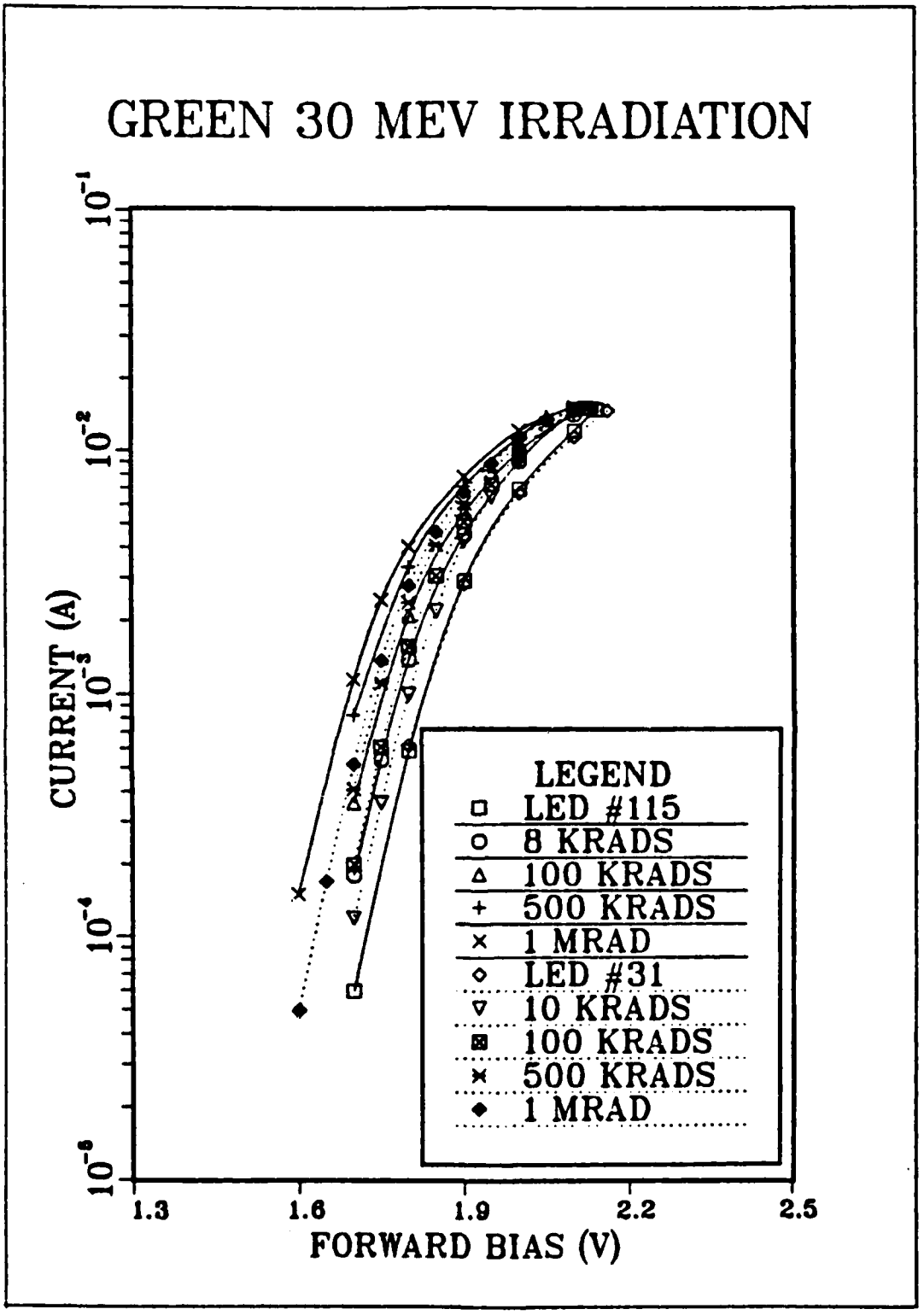

Figure 12. VI Characteristics for Green LEDs in Low Current Mode

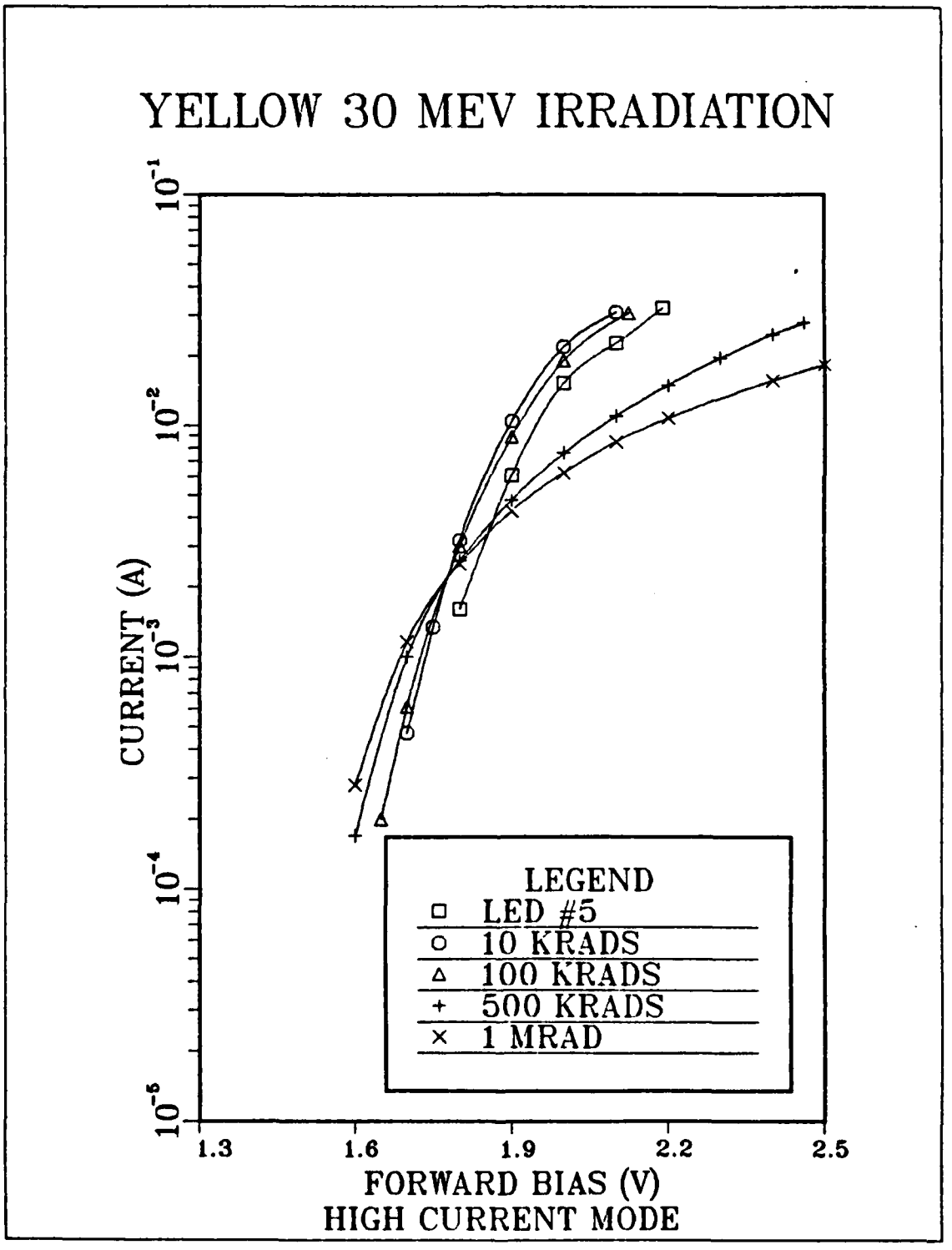

Figure 13. VI Characteristics for Yellow LEDs in High Current Mode

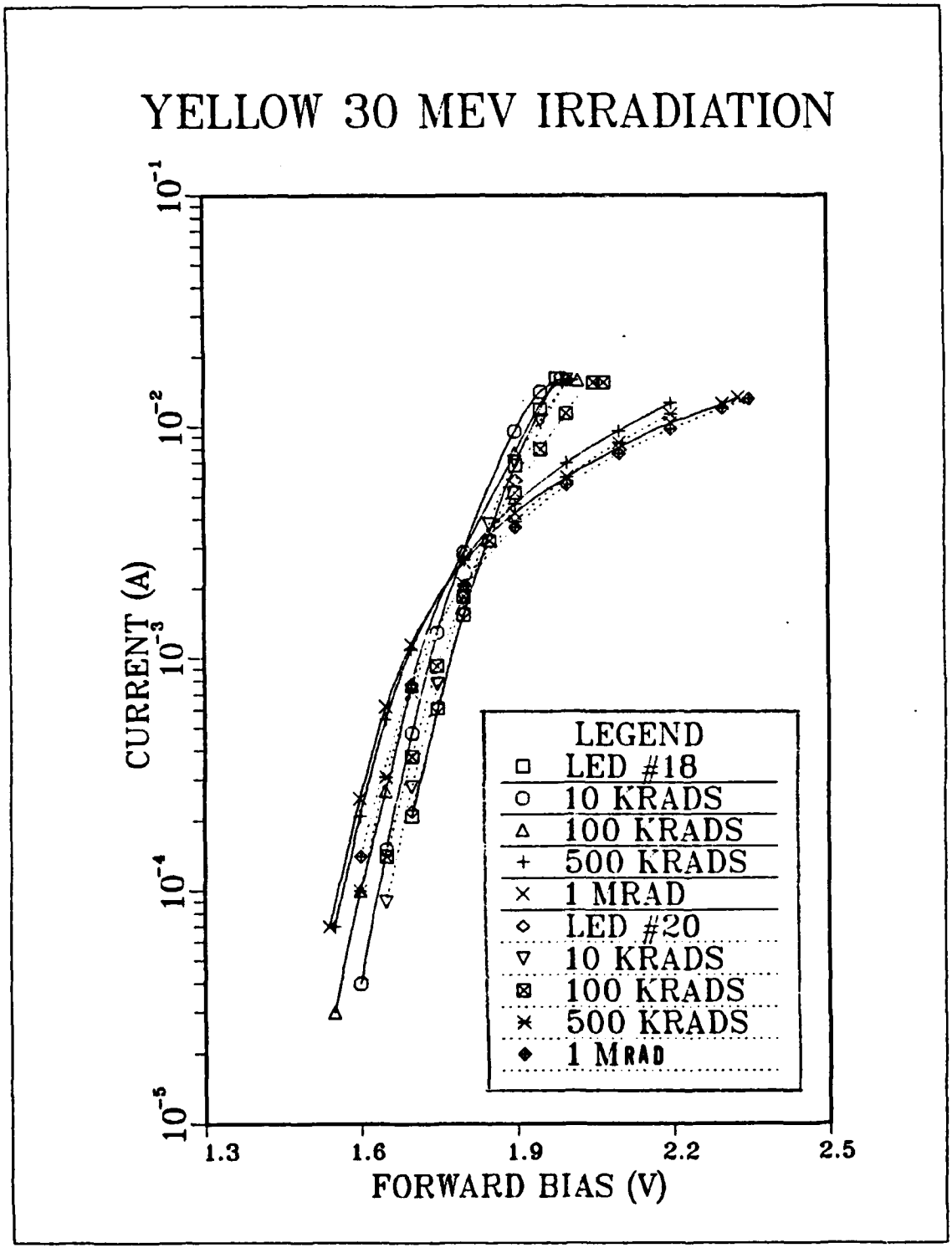

Figure 14. VI Characteristics for Yellow LEDs in Low Current Mode

line which distinguishes the curves by LED on the graphs. On graphs with only a single LED only solid lines are used.

For values used in calculating the slope, used for determining the type of current controlling mechanism, the important part of the graph is the straight part, constant slope. It can be seen that the red LED slope remained constant and HER changed very slightly. The yellow and green LEDs show a more apparent shift in slope. Above the point where the curves start to flatten or even turn downward the slope of the curve changed rather dramatically for the yellow LEDs.

The effect of temperature on n, the constant that indicates whether the current is diffusion or space charge limited, has not been quantified. As discussed, all irradiation runs were done at room temperature but the energy transferred to the LEDs by the beam could affect n slightly. However, little or no difference in V-I measurements was detected after the LEDs cooled and the measurements were redone.

Appendix A gives voltage, current and absolute output intensities for LEDs before irradiation and after total irradiation for 4.0 V and 6.0 V at the power supply. The values for post-irradiation are after 30 days to allow annealing.

The type of current controlling mechanism for each type of LED will be shown. This is the value of n from

$$J \text{ or } I = C \exp(qV_a/nkT) \tag{40}$$

where values for J are for total current as found from Figures 7 throuqh 14. Values for I are for radiative current found from the graphs as outlined in the following sections. The value of n is calculated from

$$\ln J = \ln C + \frac{qV_a}{nkT} \tag{41}$$

and

$$\Delta(\ln J) = \frac{q}{nkT} \Delta V_a \tag{42}$$

or

$$n = \frac{q}{kT} \frac{\Delta V_a}{\Delta(\ln J)} \tag{43}$$

The values for n are tabulated in Table VI. The values given in Table VI are the LED color and serial number and the LED power supply voltage. If the power supply voltage is 6.0 V then the LED is being powered in the high current mode. This is only a relative designation and is not a special mode of operation. The three values of n are as follows: (a) n_o represents the value of n for the LED before irradiation, (b) n_I represents the value of n for the LED after all irradiation, (c) n_{ex} represents the value of n

for the excess current induced. This was calculated by taking the difference of the values of J for a given V_a at different points on the curve and calculating n in the same manner given above. It is for the value after total irradiation. Note that the values for the yellow LED's vary greatly due to the difficulty in measuring the slope of the VI curve when the shape was changing so much.

There are several sources of error in the values in addition to the temperature effects already discussed. Due to the limitations of equipment (multimeters), it was not always possible to get well down onto the "straight" portion of the curve. Because the curves are semi-log, the slope measurements are very sensitive to slight changes. Additionally, the curves bend over at the top due to reaching an overdriven state where the equation no longer holds.

Examination of Table VI shows that the high efficiency red (HER), green, and yellow LEDs show space charge characteristics before and after irradiation and that the excess current induced by irradiation was space charge type. The yellow values were particularly hard to measure due to the overdriven state reached at relatively low values of V_a as seen in Figures 13 and 14. The red LEDs show total current of diffusion type and an excess current also of diffusion type. This indicates that the red LEDs were

TABLE VI

VALUES OF n FOR TOTAL CURRENT, J

LED Color	Serial Number	Power Supply (V)	n_0	n_I	n_{ex}
RED	#66	4.0	1.5	1.3	1.1
		6.0	1.6	1.3	1.0
	#63	4.0	1.5	1.3	1.0
		6.0	1.4	1.3	1.1
	#65	4.0	1.5	1.3	1.3
HER	#80	4.0	2.0	2.4	3.0
		6.0	2.7	2.4	2.2
	#92	4.0	2.0	2.1	2.2
		6.0	2.2	2.1	2.0
	#91	4.0	2.0	2.9	3.7
GREEN	#115	4.0	1.7	2.1	2.3
		6.0	3.0	3.6	3.9
	#42	4.0	1.7	2.2	2.3
		6.0	2.4	3.9	6.5
	#31	4.0	1.9	2.3	2.9
YELLOW	#18	4.0	2.3	2.5	17.3
		6.0	1.8	3.6	---
	#5	4.0	2.8	5.6	---
		6.0	7.7	26	66
	#20	4.0	2.0	2.3	9.5

n_0 = Value before irradiation

n_I = Value after irradiation

n_{ex} = Value for excess current induced

probably being driven at a higher current density and possibly had smaller junction diameters. Examination of Figures 7 and 8 shows that the red LEDs also showed less tendency to being overdriven to a higher level compared to the starting value of the curve. The HER curves also show the characteristics of higher current density similar to the red LEDs. The higher current density in the red and HER could be a result of smaller junction area, more efficient carrier diffusion or both. This was not further investigated.

D. LED LIGHT OUTPUT DEGRADATION

The second type of measurements taken were for light output intensity versus dose or fluence for the LEDs. Real time measurements were taken using a photocell in the target chamber. Measurements of absolute output intensity were also obtained using the Fiber Optics 550 meter. The results for the real time measurements are shown in Figures 15 through 30 and the results for the absolute values are tabulated in Appendix A.

Figures 15 through 26 show a normalized light output (I/I_0) versus time. Each color LED has three sets of graphs. One shows the high current mode, one shows the two LEDs at the lower current values and one shows all three LEDs for a given color plotted together. The flux for all runs averaged to 4.3×10^{11} e^-/cm^2-s as shown on the graphs

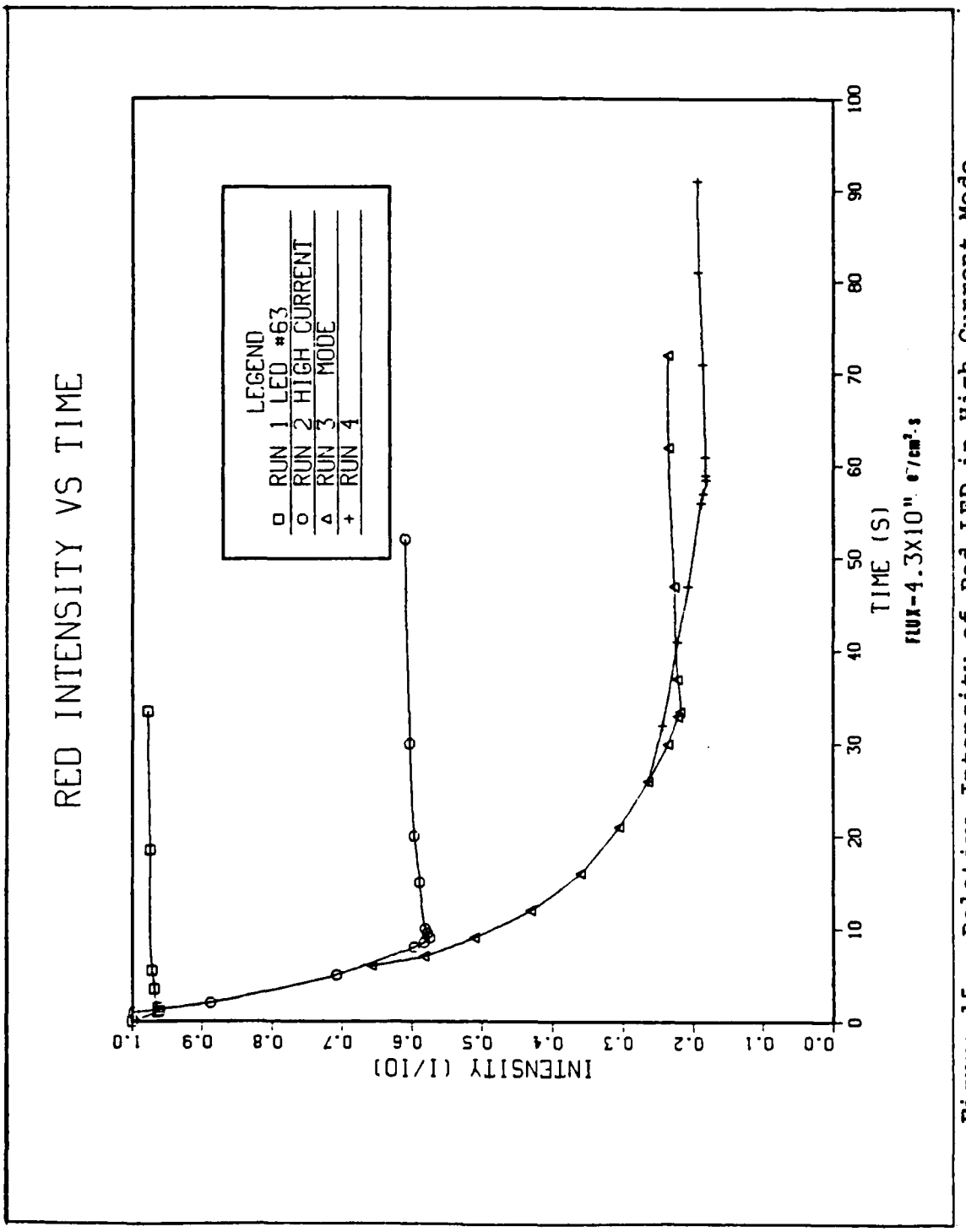

Figure 15. Relative Intensity of Red LED in High Current Mode

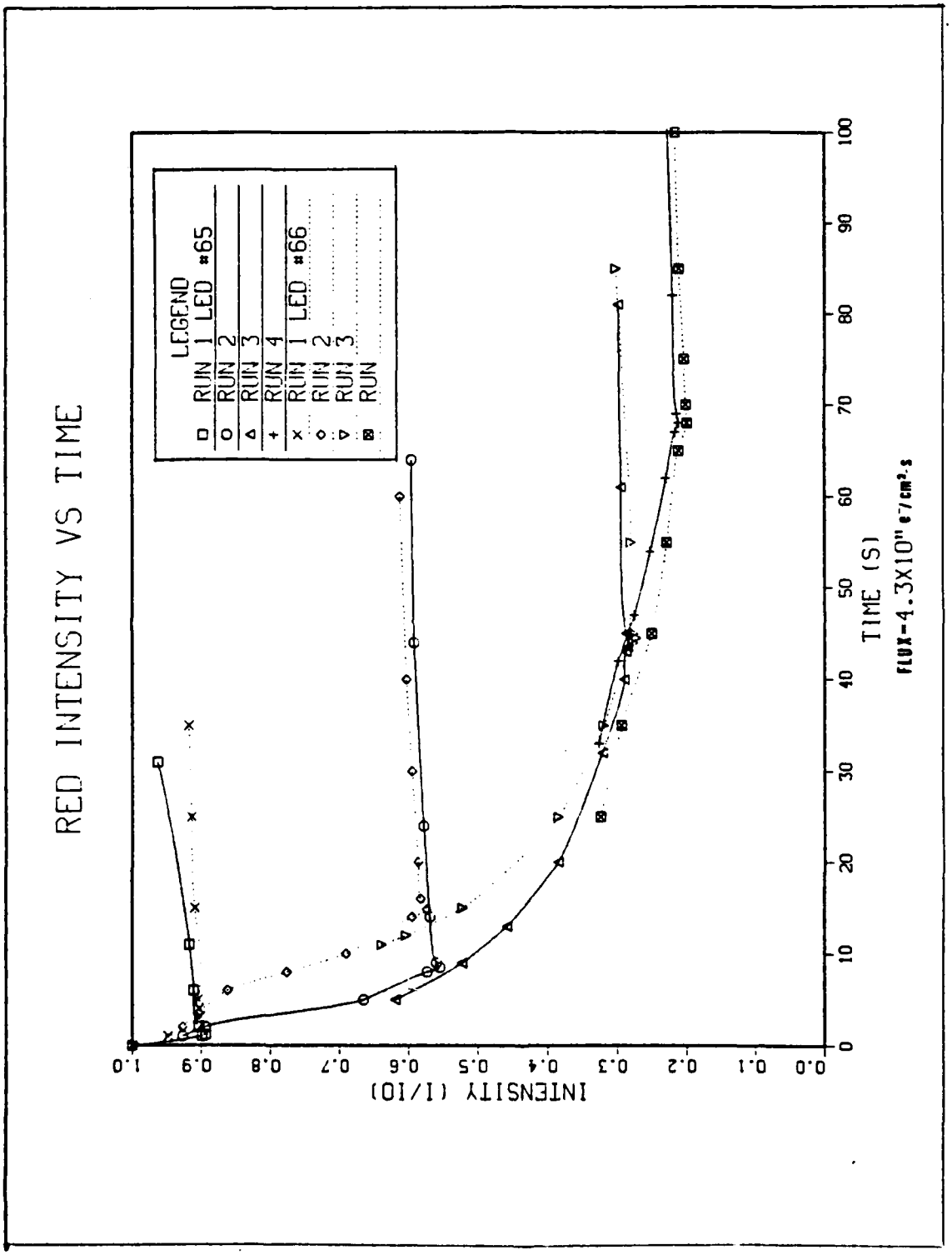

Figure 16. Relative Intensity of Red LEDs

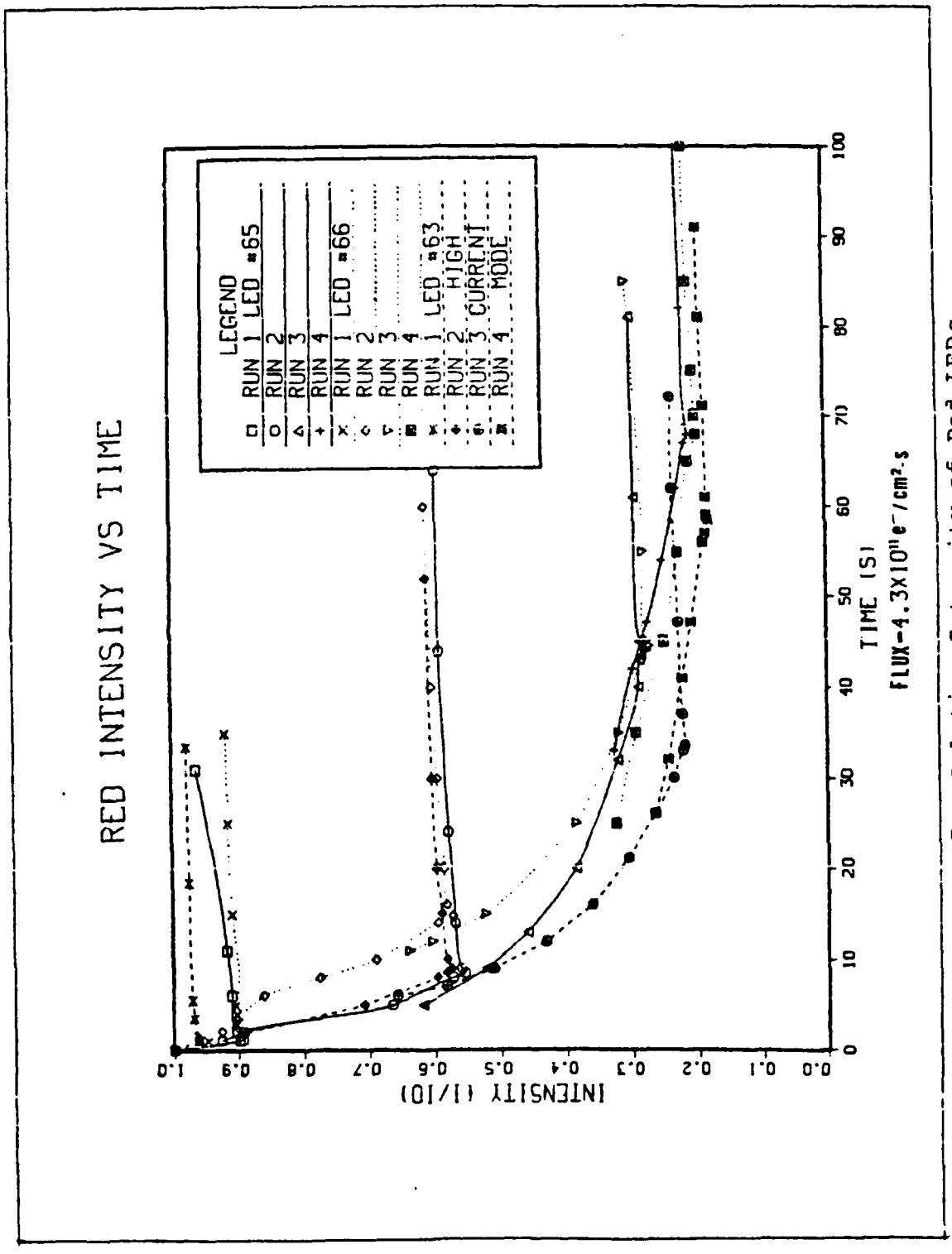

Figure 17. Relative Intensity of Red LEDs

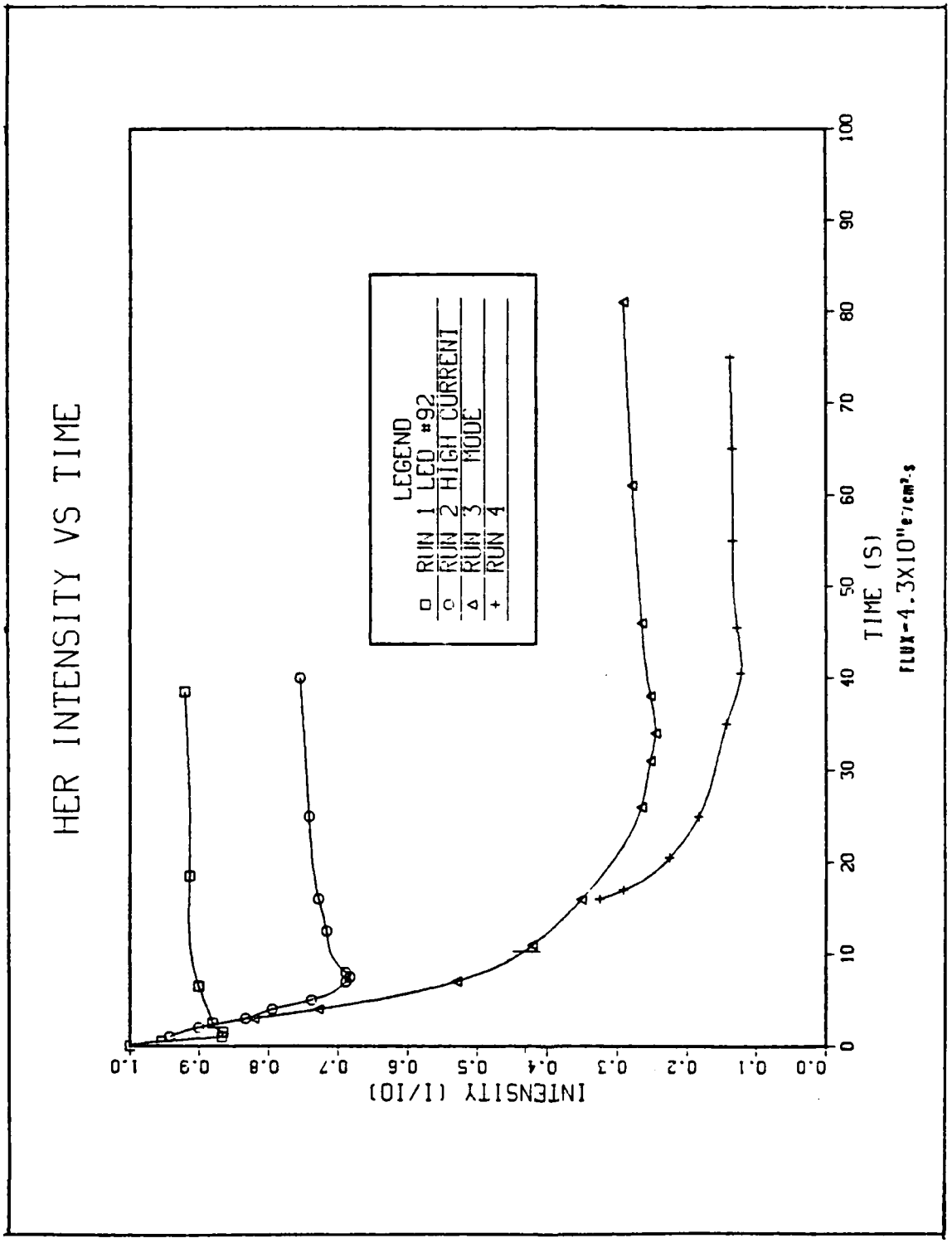

Figure 18. Relative Intensity of High Efficiency Red LED in High Current Mode

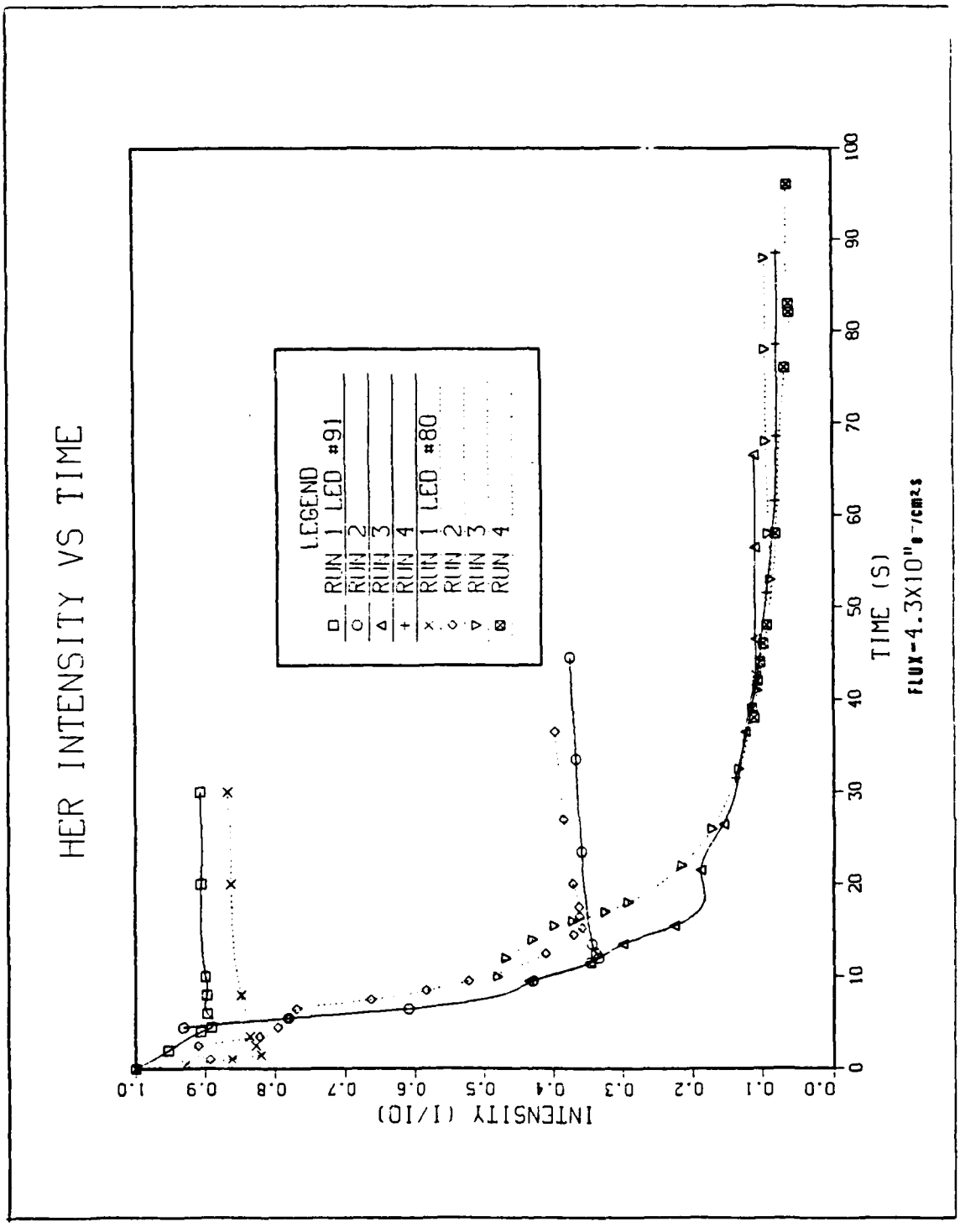

Figure 19. Relative Intensity of High Efficiency Red LEDs

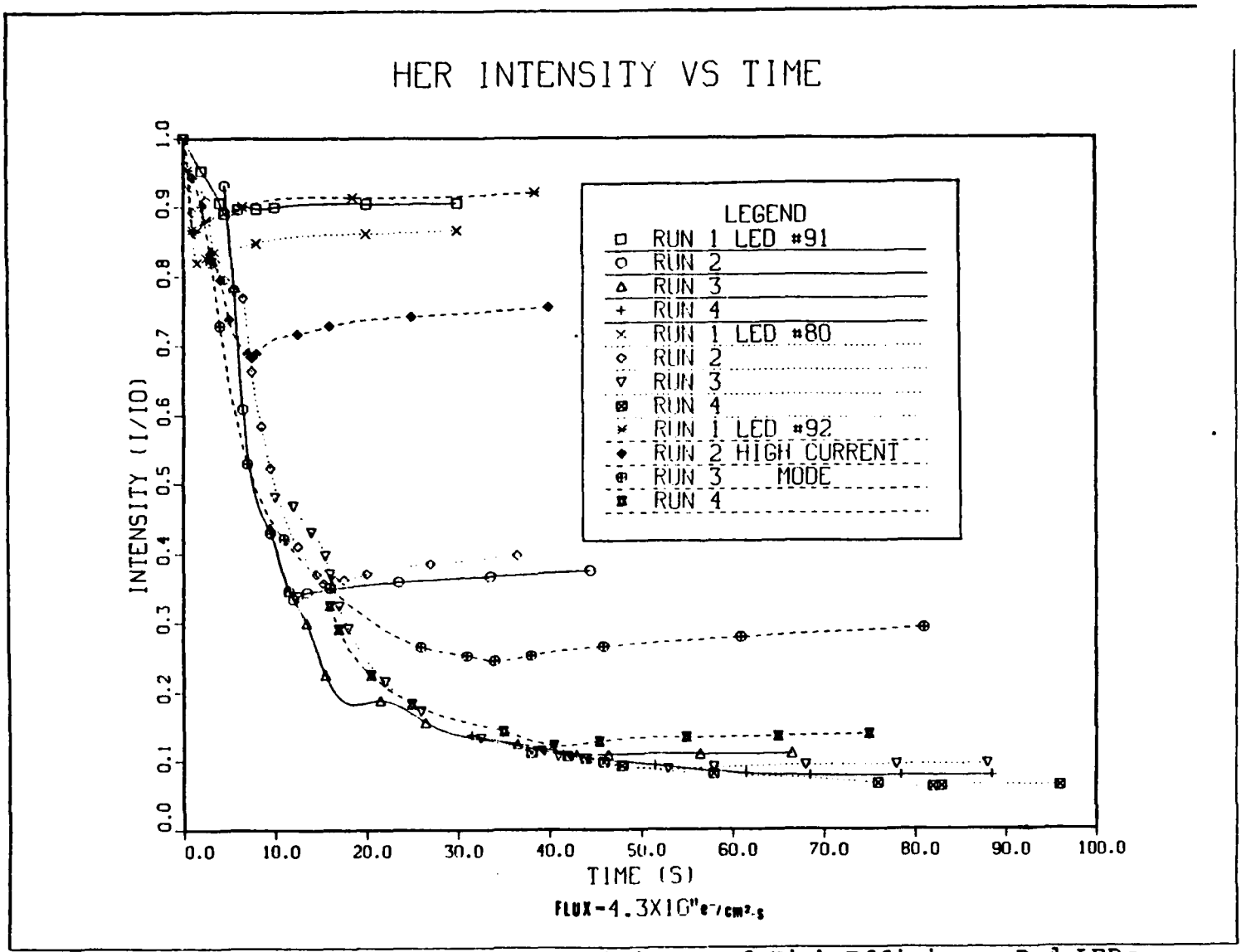

Figure 20. Relative Efficiency of High Efficiency Red LEDs

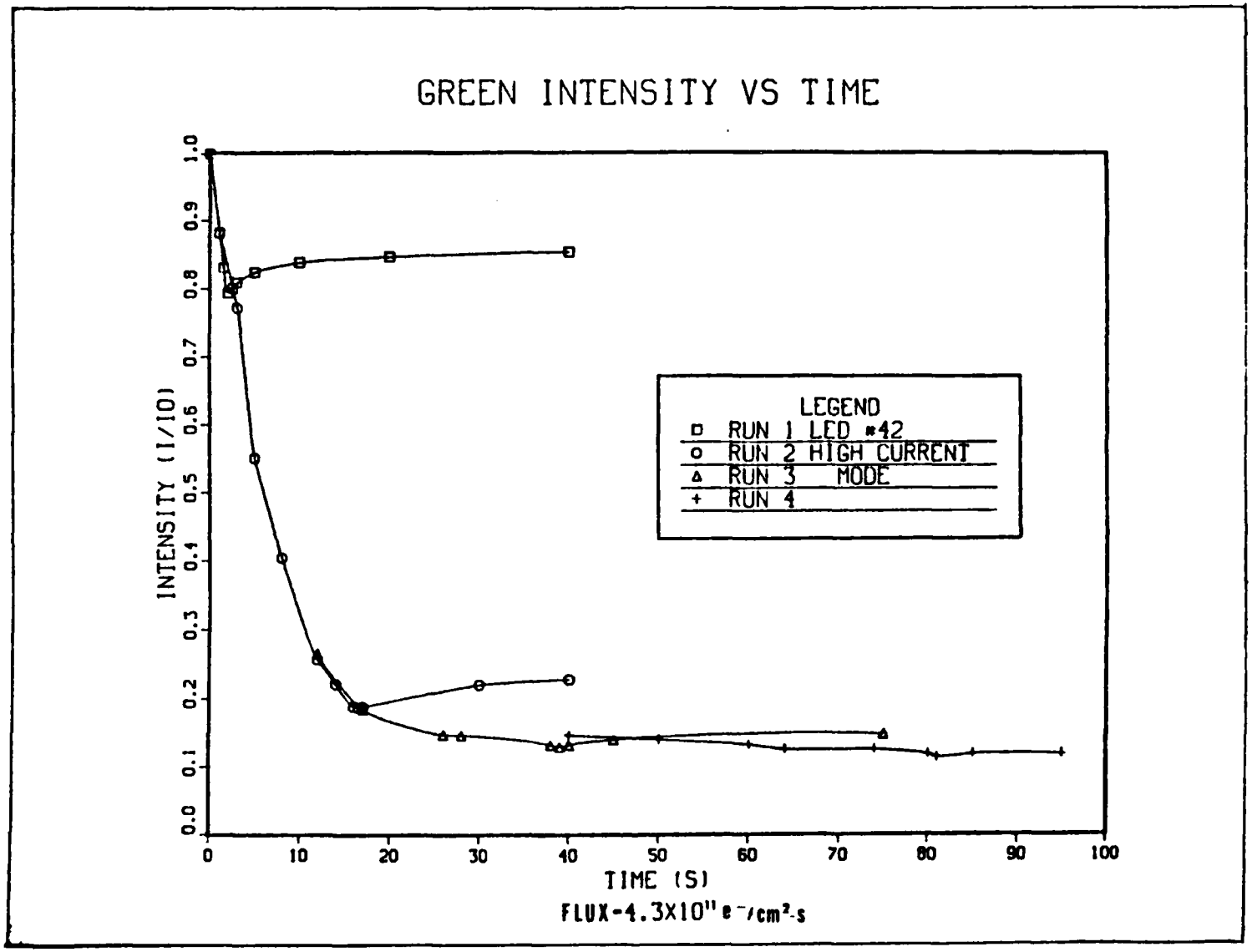

Figure 21. Relative Intensity of Green LED in High Current Mode

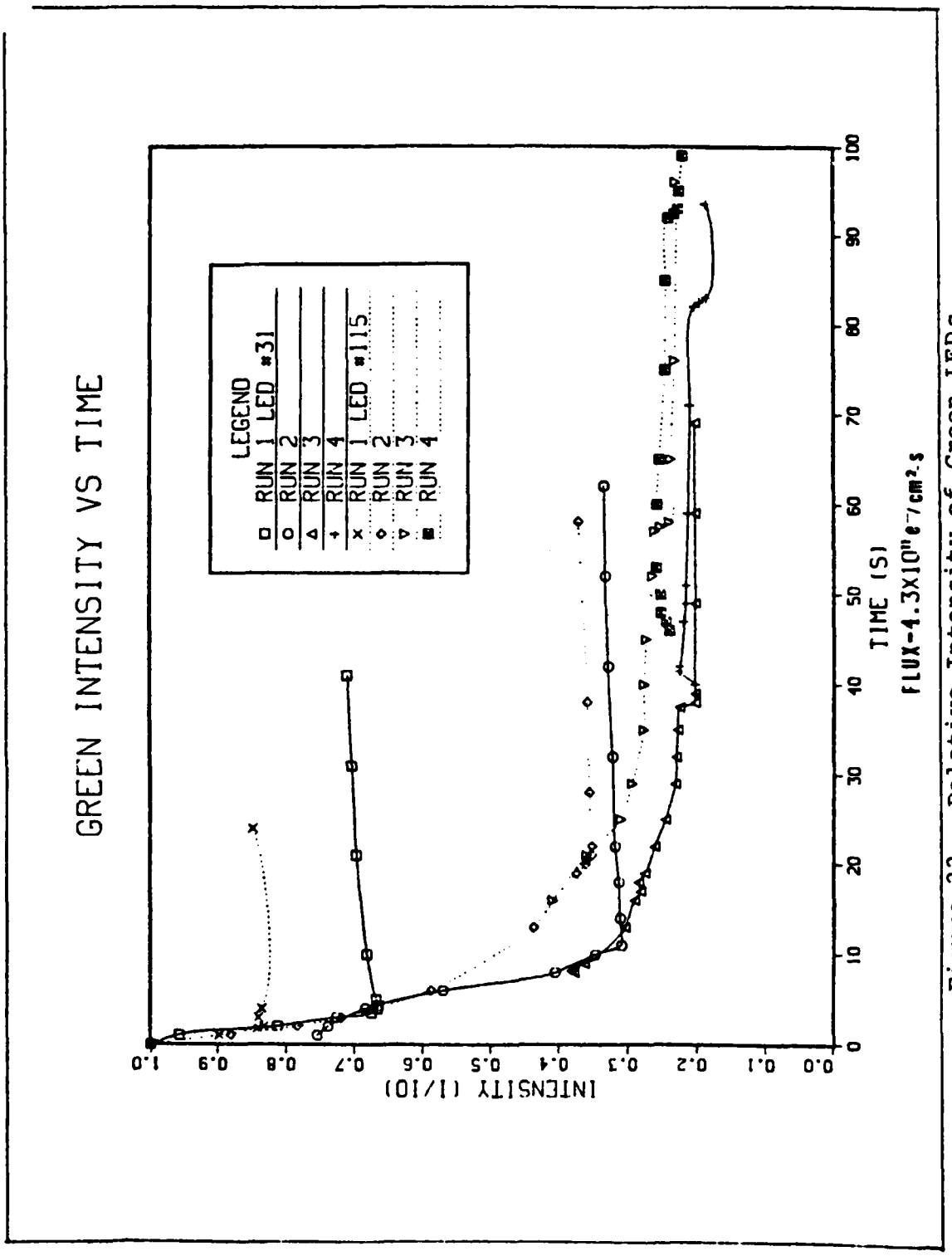

Figure 22. Relative Intensity of Green LEDs

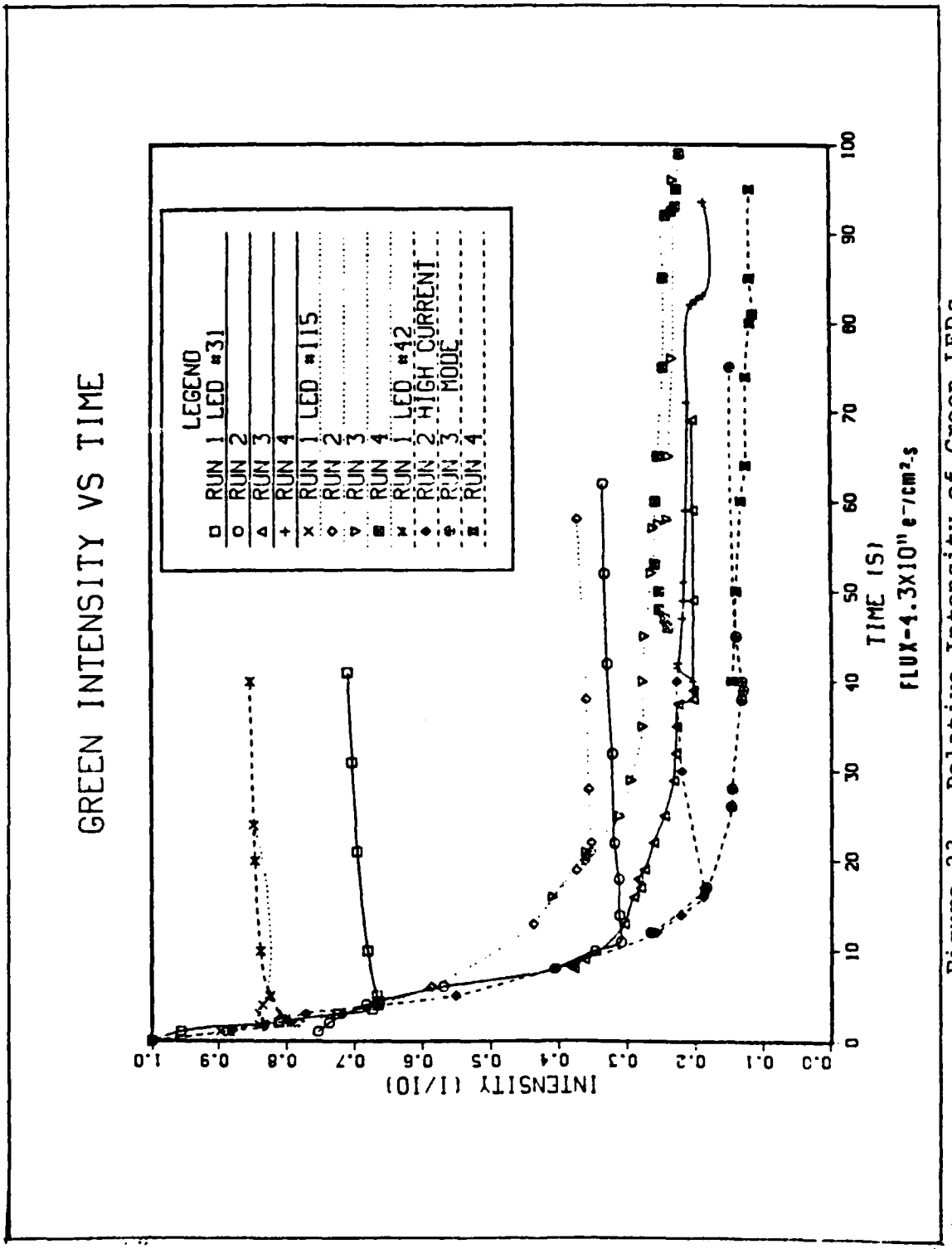

Figure 23. Relative Intensity of Green LEDs

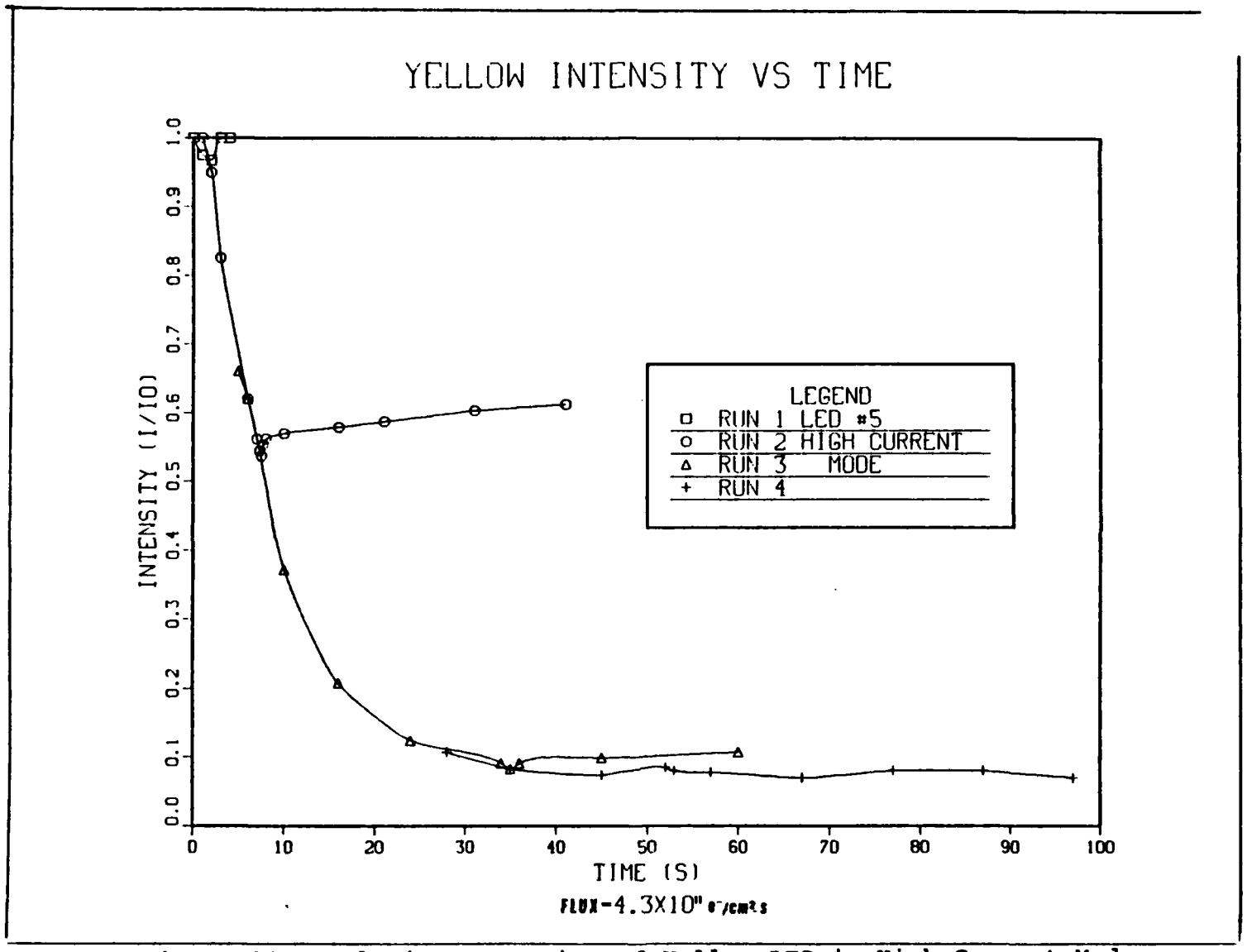

Figure 24. Relative Intensity of Yellow LED in High Current Mode

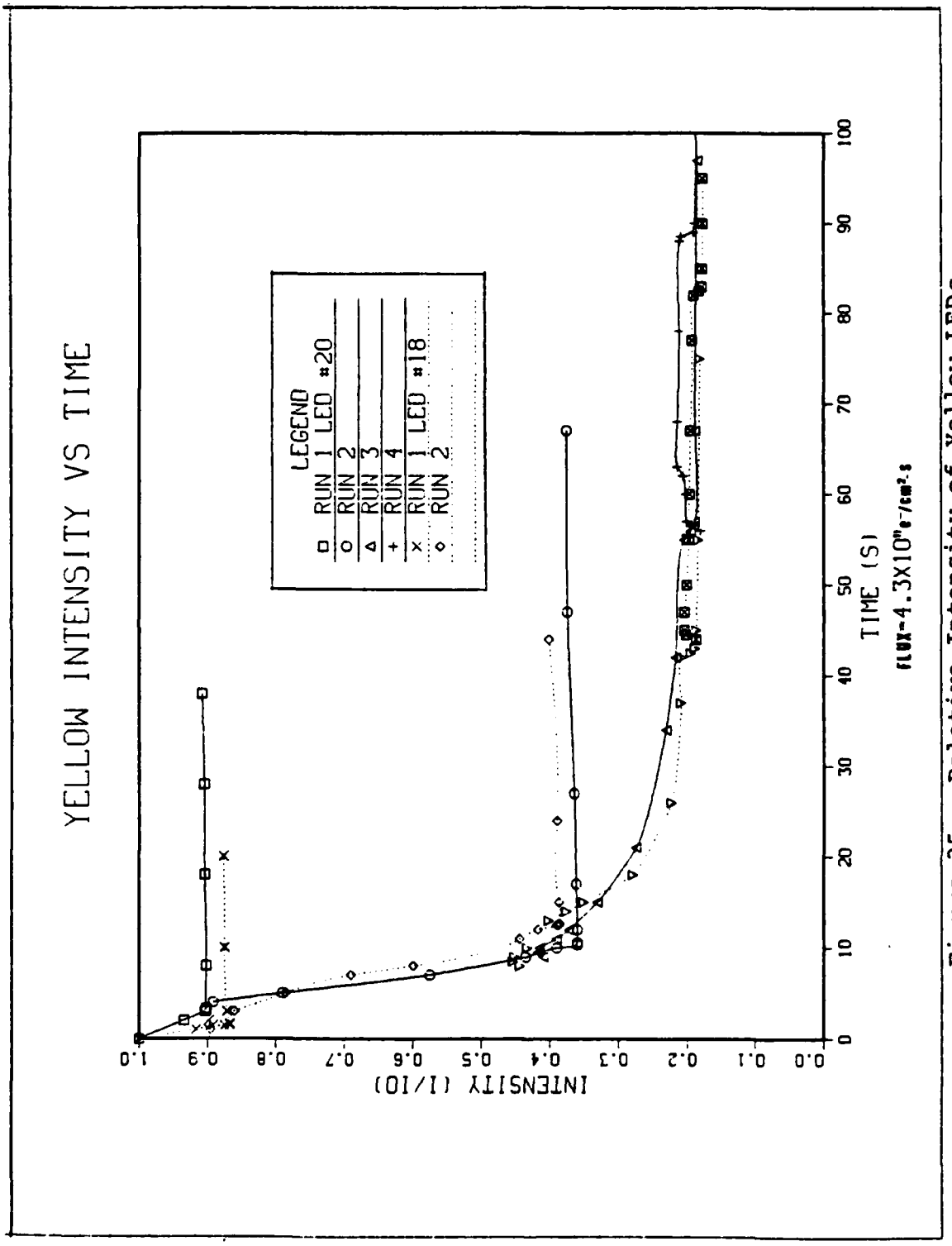

Figure 25. Relative Intensity of Yellow LEDs

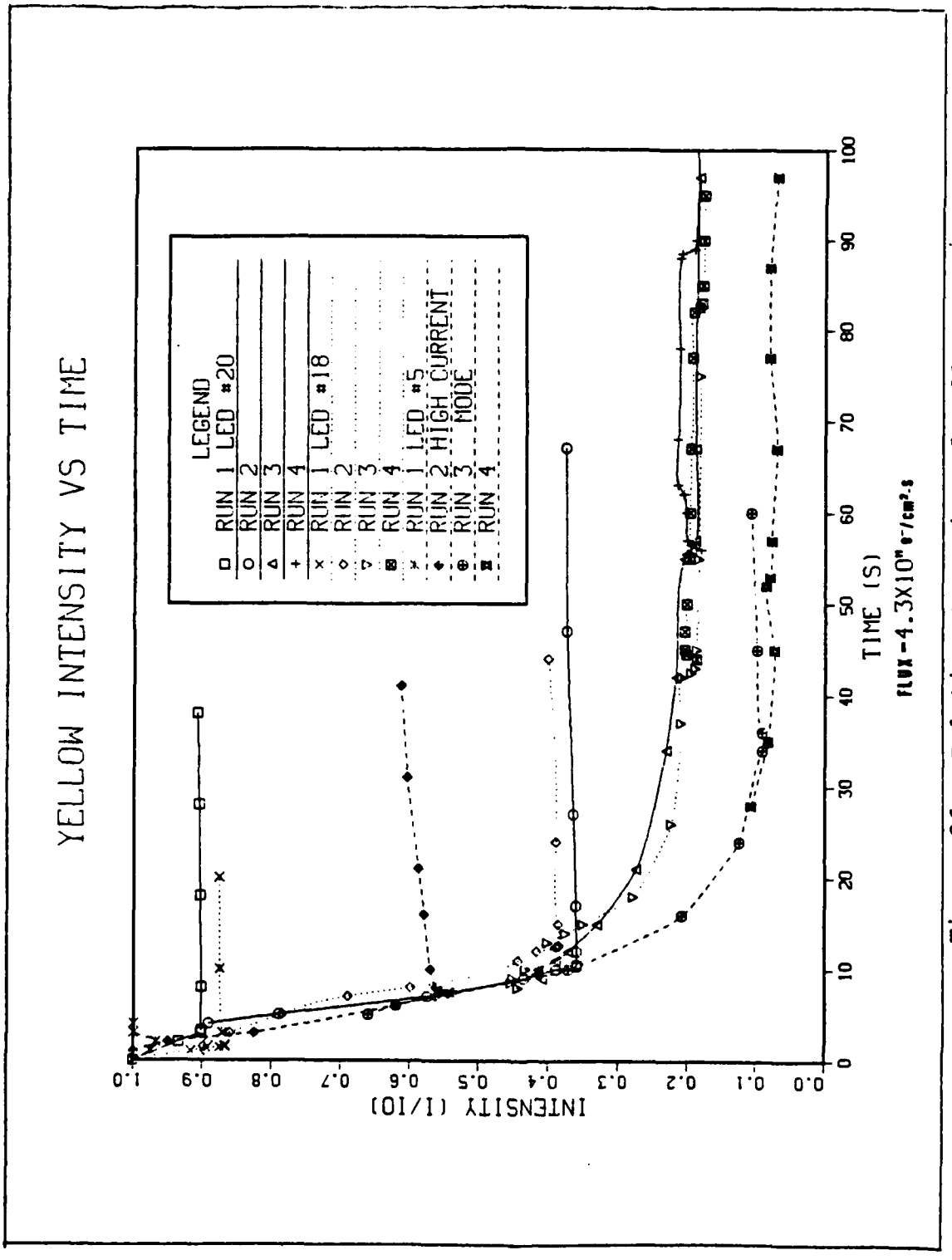

Figure 26. Relative Intensity of Yellow LEDs

and although there was some variation (1.2×10^{11} e^-/cm^2-s to 6.2×10^{11} e^-/cm^2-s) in the beam this average value is used on all of the graphs. In Figures 15 through 26 the decrease in output intensity is seen by the downward trend of the plot for each LED. This decrease in intensity has an approximately constant slope with time and the sustained fluence increase until the device is no longer giving significant light output.

Figures 27 through 30 show the output intensity versus fluence. The fluence was obtained by multiplying flux times time, using the average value for the flux.

On both types of plots, indications of annealing can be seen. On the first type of graph, the curves show a sharp downward slope until the point where the LINAC electron beam was switched off. The line of intensity versus time then slopes up sharply at first, flattening out but still with a positive slope for an extended period of time. The time between each run was about five minutes. The total amount of recovery can be gauged by comparing the bottom part of the dip to the first value on the next run. The second set of curves have the annealing tails cut off so that the difference between the end of one run and the beginning of the next is more readily seen.

The annealing properties of GaAs and GaP and $GaAs_xP_{1-x}$ are known phenomenon that make them useful materials. This

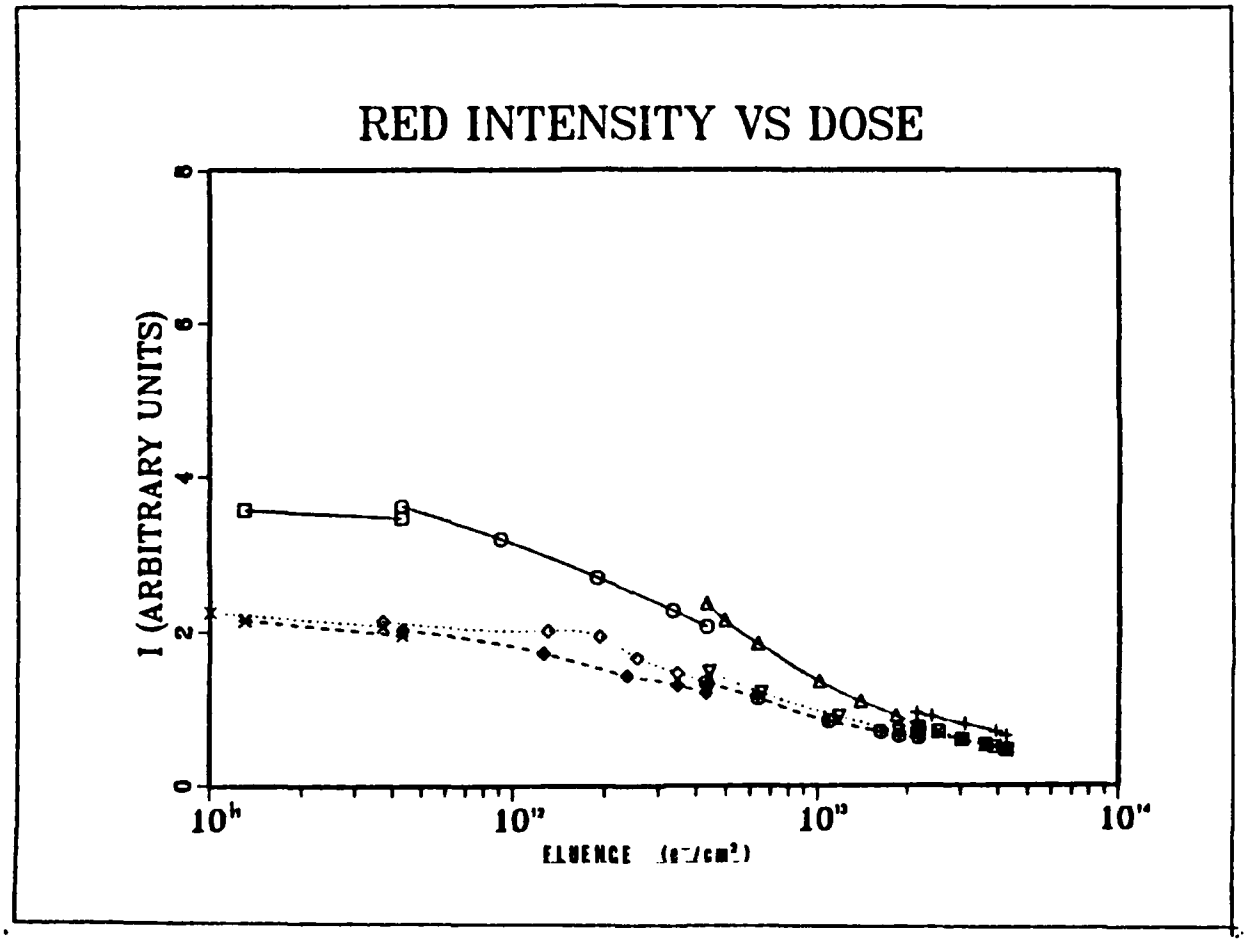

Figure 27. Intensity of Red LED's. Solid Lines Indicate High Current Mode

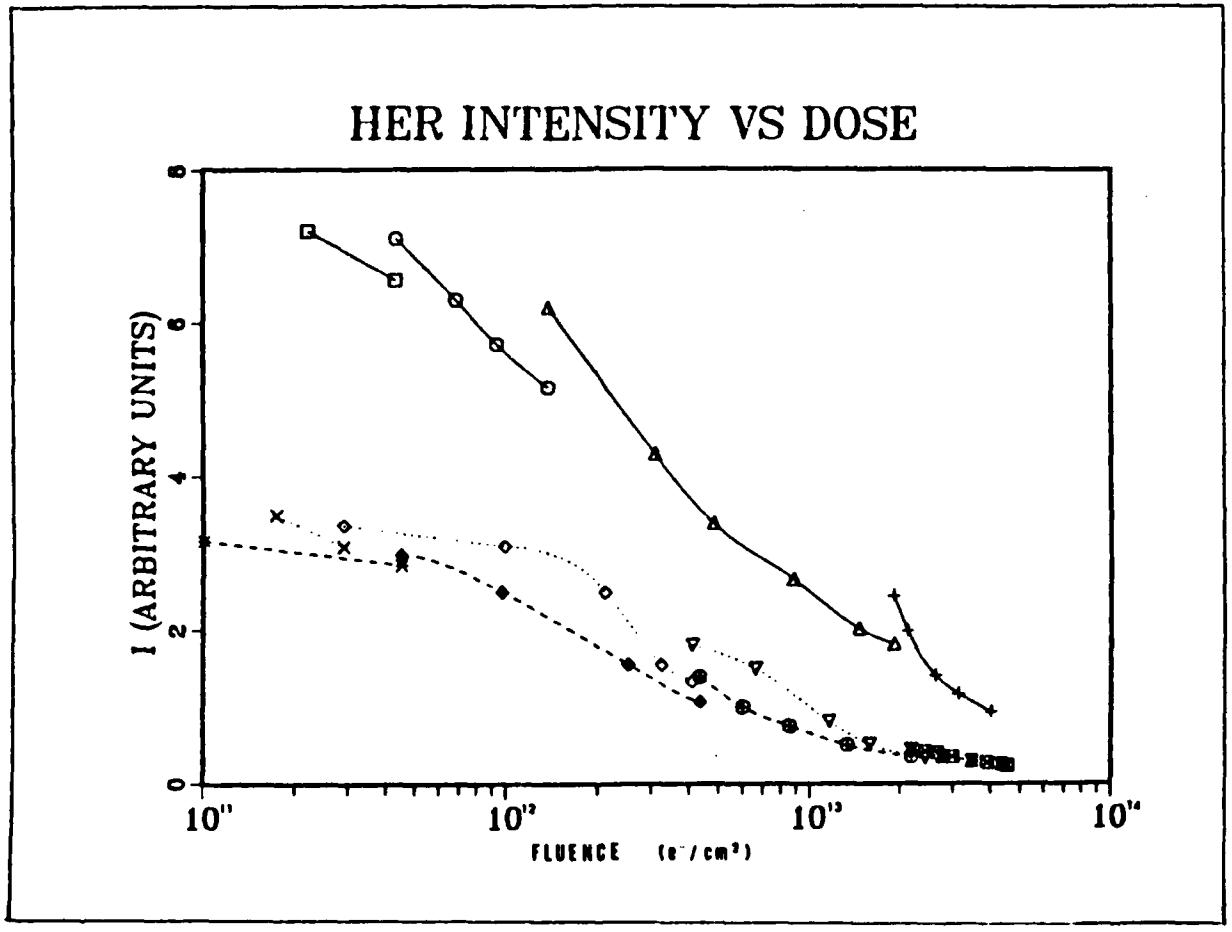

Figure 28. Intensity of High Efficiency Red LEDs. Solid Lines Indicate High Current Mode.

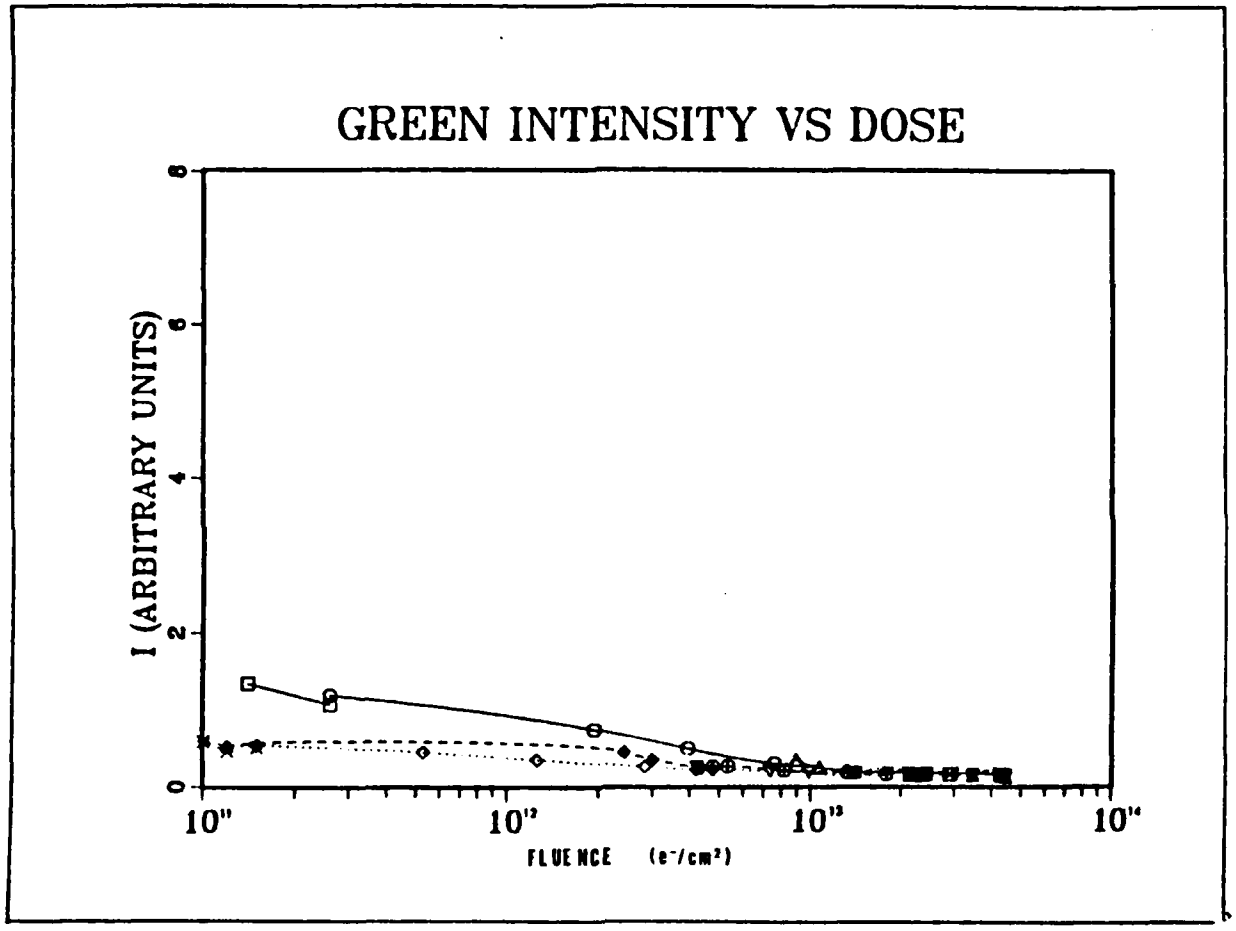

Figure 29. Intensity of Green LEDs. Solid Lines Indicate High Current Mode.

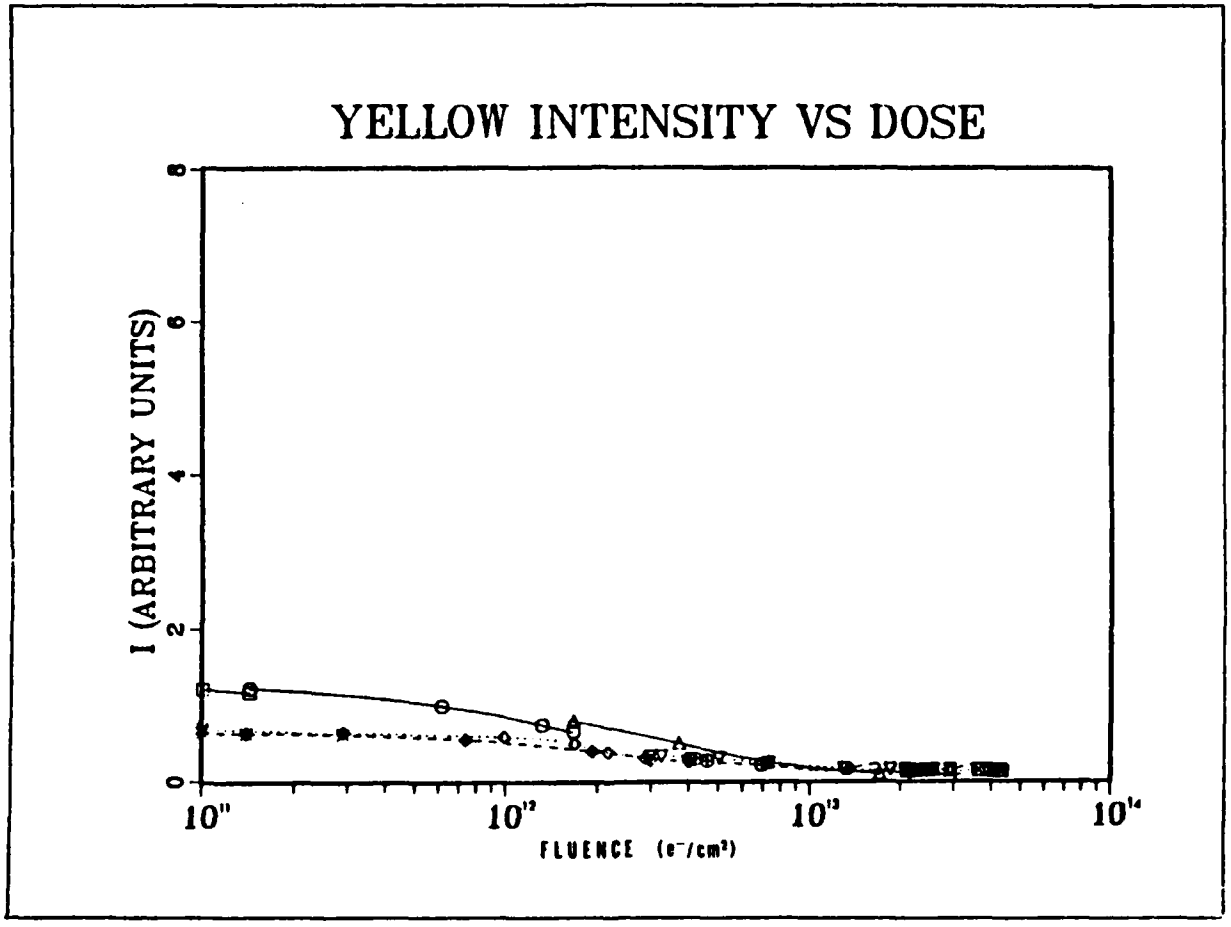

Figure 30. Intensity of Yellow LEDs. Solid Lines Indicate High Current Mode.

is one reason NASA suggested GaAs for the solar power satellite as mentioned. No attempt is made here to quantify the values.

An interesting and unexpected phenomenon can be seen on the graphs for the yellow and green LEDs. On the last runs, where the LED is essentially "dead", the output intensity was raised during the time that the electron beam was on. This effect was noticeable on the TV monitor where the visible LED output glow was seen to increase during irradiation. Sometimes no visible emission at all existed before and after the electron beam was on and a visible glow did appear during irradiation. Notice also the effect was not as pronounced for the high current mode of operation and was not detected in the red and HER LEDs. This phenomenon was not further investigated.

The values for n for the radiative current were calculated in a manner similar to that done for total current. The values used for getting the slope of the curve are those for the absolute output of the LEDs given in Appendix A. These values are listed in Table VII. It should be emphasized that the values for n in this table are for that portion of the current which is radiative, in other words producing light. The radiative current controlling mechanism can be different from the total current controlling mechanism, and is in several cases. The values in

TABLE VII

VALUES OF n FOR RADIATIVE CURRENT

LED Color	Serial Number	Power Supply (V)	n_0	n_I
RED	#66	4.0	1.1	1.1
		6.0	1.2	1.1
	#63	4.0	1.1	1.1
		6.0	1.1	1.1
HER	#80	4.0	1.2	1.8
		6.0	1.7	1.8
	#92	4.0	1.2	1.5
		6.0	1.2	1.5
GREEN	#42	4.0	1.8	2.8
		6.0	1.8	3.2
	#115	4.0	2.0	2.8
		6.0	2.1	3.2
YELLOW	#18	4.0	1.8	5.6
		6.0	1.9	6.9
	#5	4.0	1.9	5.6
		6.0	2.1	5.6

n_0 = Value before irradiation

n_I = Value after irradiation

the table are n_0 for before irradiation and n_I for after irradiation.

The red and HER LEDs appear to have radiative current that is diffusion controlled. The yellow and green LEDs have radiative current that is space charge recombination controlled.

E. LIFETIME-DAMAGE CONSTANT PRODUCTS

As discussed in the background chapter and summarized in Table IV, if one knows the current controlling mechanism for an LED, a phenomenological lifetime-damage constant product, t_0K, can be determined. The previous sections concerned determination of the current controlling mechanism by determination of n, the slope of the V-I and V-J curves. These current controlling mechanisms and the calculated τ_0K value are tabulated in Table VIII.

In using the appropriate equation from Table IV, the value of I/I_0 is needed. This was obtained from the appropriate curve in Figures 15 through 26 for I/I_0 at 10 seconds. This value was chosen because it appears to be a point where the curves start to flatten and the formerly constant values for τ_0K are changing. Thus for LED #63 the value is $I/I_0 = .48$ and from Table IV for I and J diffusion controlled

$$[(I_0/I)^{2/3} - 1] = \tau_0 K \Phi \qquad (44)$$

TABLE VIII

LIFETIME-DAMAGE CONSTANT PRODUCTS FOR 30-MeV ELECTRON IRRADIATION

Color Diode	Serial Number	Power Supply (V)	Material	Current Controlling Mechanism	$\tau_0 K (10^{-13} cm^2/electron)$
RED	#63	6.0	$GaAs_{.4}P_{.6}$ on GaAs Substrate	I: Diffusion	1.5
	#65	4.0		J: Diffusion	1.4
	#66	4.0			1.1
HER	#92	6.0	$GaAs_{.35}P_{.65}$ on GaP Substrate	I: Diffusion	0.8
	#91	4.0		J: Space Charge	0.8
	#80	4.0			0.6
GREEN	#42	6.0	GaP on GaP Substrate	I: Space Charge	9.7
	#31	4.0		J: Space Charge	3.5
	#115	4.0			5.9
YELLOW	#5	6.0	$GaAs_{.1}P_{.9}$ on GaP Substrate	I: Space Charge	2.0
	#20	4.0		J: Space Charge	1.7
	#18	4.0			2.0

and $\Phi = 4.3 \times 10^{12}$ e^-/cm^2 so that

$$\tau_0 K = 1.5 \times 10^{-13} \text{ cm}^2/e^- \quad (45)$$

Since the green and yellow LEDs were totally space charge recombination controlled, values for J instead of I are used. The values for J and J_0 were taken at the same voltage for a given color at a point in the middle of the flat part of the slope.

Note that the value of $\tau_0 K$ is inversely related to the hardness of the device. Thus the higher the number the more susceptible is the device to radiation damage from 30-MeV electrons. The high efficiency red LEDs appear to be the hardest with the red and yellow LEDs slightly more susceptible. The green LEDs are significantly softer than the other three types of LEDs.

F. DISCUSSION

The lifetime-damage constant products shown in Table VIII for 30-MeV electron irradiation of the LEDs are appropriate for constant current operation of these devices. Stanley [Ref. 4] tested epitaxial (not specified if liquid or vapor) GaAs LEDs and found $\tau_0 K$ values in the range of 1-2 $\times 10^{-13}$ cm^2/electron for irradiation by high energy electrons. His values for diffused LEDs were (.12-.15) $\times 10^{-13}$ cm^2/electron for GaAs and .04 $\times 10^{-13}$ cm^2/electron for GaP.

Rose and Barnes [Ref. 8] showed that proton irradiation of LEDs resulted in an increase in total LED current at a given voltage. This nonradiative excess current was a space charge recombination current which degraded the LED output for constant current operation. For higher-current-density small-junction-area LEDs the total current (radiative and nonradiative) was closer to a diffusion current where n = 1, and the proton induced excess current was less significant over a large voltage range. They compared their results to earlier work they had done using neutrons and found similar effects. The results of my experiment for 30-MeV electron irradiation showed a similar increase in total current for irradiation. Three of the four types tested had an excess nonradiative current that was space charge recombination dominated similar to the Rose and Barnes results. One group of LEDs showed behavior similar to the higher-current-density small-junction-area devices tested by Rose and Barnes. It is not certain which characteristic determined this behavior although a smaller junction area is assumed.

All the LEDs tested here proved to have similar sensitivity to radiation with values close to earlier tests on epitaxially fabricated LEDs. The green LEDs, the only color LEDs fabricated by LPE are more sensitive than the other colors which are products of VPE.

Rose and Barnes [Ref. 8] suggest that bias induced annealing in LEDs indicates that damage consists primarily

of point defects rather than damage clusters which are characteristic of neutron induced damage. They and Millea and Aukerman [Ref. 6] observed the absence of bias induced recovery in neutron irradiated LEDs. This is in agreement with the fact that the average energy transferred by an energetic electron undergoing collision is much less than that produced by an energetic neutron undergoing collision. Usually an electron will produce in effect one product electron in one collision and then pass on. A neutron must collide with the nucleus, a much smaller target, in essentially an elastic collision. This displaces the nucleus which ionizes nearby lattice atoms causing a cluster of local defects.

Ionizing proton damage usually produces point defects. Of interest, Hardwick and Kalma [Ref. 16] tested a variety of LEDs using 30-MeV protons and found the device to degrade 50% after 2×10^{11} protons/cm^2. This converts to a $\tau_0 K$ of 0.29×10^{-13} cm^2/proton which is approximately an order of magnitude smaller than the values obtained in this experiment.

V. CONCLUSIONS AND FUTURE WORK

This investigation of electron damage in LEDs has shown that the effects of 30-MeV electron irradiation are similar to those of earlier work for electrons and for other radiation mechanisms.

The LPE fabricated LED showed a higher vulnerability to damage than the VPE LEDs. The red and HER LEDs were slightly more resistant to damage than the yellow. In the case of the red LEDs, this appears to be due to a higher current density due to a smaller junction size. In the case of an HER LED it could be due to the same effect, although its current density doesn't appear to be as high as the red's. It could also benefit from the higher efficiency in conversion (nonradiative to radiative current ratio). In other words, although its total current density is not as high as that of the red LED, its radiative current density is higher.

There are two electron induced degradation components in constant current operation of LEDs. Firstly, introduction of defect related, nonradiative recombination centers degrades the minority carrier lifetime and light output through increased competition for excess carriers. Secondly, excess current due to additional recombinations at

defects in the space charge regions can cause an increase in LED current and a reduction in efficiency. The second type can possibly be detected by conducting the irradiation at a constant voltage instead of constant current, as suggested by Rose and Barnes [Ref. 8]. There are some indications that this effect is present since the red LEDs showed less spread in the voltage current characteristic curves. Indications in the other colors of LEDs were not conclusive. It should be noted that the longer wavelength devices showed more hardness. This effect could well extend into the infrared region.

In future work, closer attention might be paid to temperature variation due to absorbed energy possibly by using a heat sink or liquid nitrogen bath. Additionally, the dosimetry variations due to beam distribution might be determined by aiming the beam through various size holes in phosphorescently painted material and measuring the intensity variation. The problem of secondary gamma and electron production could be reduced by cutting off the metal can surrounding the active part of the diode and positioning a dosimeter next to the active region. This would give a more precise measurement of the effects of electrons on the semiconductor material itself. On the other hand, with the experiment performed as here, the effect on the total device is found, also a useful piece of

information. Fine tuning dosimetry is a difficult task and one fraught with many interpretive harzards. The interesting glow produced in the green and yellow LEDs might be further investigated to determine its source and why the effect is not apparently present in the red and HER LEDs.

These LEDs are designed for use in systems that are going to be used by personnel. The dosages inflicted on the devices were sufficient to cause injury or death to humans if sustained as a whole-body dose. Thus the LEDs are adequately hardened for tactical levels. These devices would not likely be hardened sufficiently for expected levels of radiation in an outer space or strategic environment but it is expected that they would find little application in an unmanned system.

APPENDIX A

LED VOLTAGE VERSUS CURRENT VERSUS LIGHT INTENSITY (USING THE FIBEROPTICS 550 METER)

A. GREEN LEDs

1. #42

	Before Irradiation		After Irradiation	
	(a) 4.0 V at power supply			
V_f(V)	J(ma)	(μW)	J(ma)	I(μW)
1.9	2.92	.34	5.85	.02
1.8	0.59	.04	2.13	.005
1.7	--	--	.36	.002
	(b) 6.0 V at power supply			
1.9	3.02	.35	5.89	.02
1.8	.62	.04	2.21	.006
1.7	--	--	.43	.002

2. #115

	(a) 4.0 V at power supply			
1.9	2.89	.28	5.29	.02
1.8	.59	.04	1.91	.005
1.7	.06	.02	.30	.002
	(b) 6.0 V at power supply			
1.9	1.60	.13	5.28	.02
1.8	.45	.02	1.81	.006
1.7	--	--	.60	.003

B. YELLOW LEDs

1. #18

	Before Irradiation		After Irradiation	
	(a) 4.0 V at power supply			
V_f(V)	J(ma)	(μW)	J(ma)	I(μW)
1.9	6.75	.65	3.64	.008
1.8	1.54	.08	1.84	.004
1.7	.61	.02	.65	.003
	(b) 6.0 V at power supply			
1.9	6.85	.68	3.64	.007
1.8	1.60	.09	1.91	.004
1.7	.21	--	.65	.003

2. #5

	(a) 4.0 V at power supply			
1.9	6.03	.52	3.62	.008
1.8	1.50	.07	1.82	.004
1.7	--	--	.69	.002
	(b) 6.0 V at power supply			
1.9	6.06	.52	3.56	.008
1.8	1.61	.08	1.89	.004
1.7	--	--	.62	.002

C. RED LEDs

1. #66

	Before Irradiation		After Irradiation	
	(a) 4.0 V at power supply			
V_f(V)	J(ma)	(μW)	J(ma)	I(μW)
1.6	3.86	.95	8.5	.99
1.5	.28	.03	.43	.03
1.4	--	--	.07	.006
	(b) 6.0 V at power supply			
1.6	3.03	.69	8.92	1.07
1.5	.28	.03	.42	.03
1.4	--	--	.04	.004

2. #63

	(a) 4.0 V at power supply			
1.6	3.53	.88	7.8	1.05
1.5	.26	.03	.37	.03
1.4	.08	--	.03	.003
	(b) 6.0 V at power supply			
1.6	4.03	1.02	7.91	1.06
1.5	.26	.03	.38	.03
1.4	--	--	.04	.003

D. HER LEDs

1. #80

	Before Irradiation		After Irradiation	
	(a) 4.0 V at power supply			
V_f(V)	J(ma)	(μW)	J(ma)	I(μW)
1.7	1.6	.49	2.52	.09
1.6	.24	.02	.50	.01
1.5	--	--	.04	.002
	(b) 6.0 V at power supply			
1.7	.93	.20	2.48	.09
1.6	.22	.02	.49	.01
1.5	.07	--	.04	.002

2. #92

	(a) 4.0 V at power supply			
1.7	1.53	.53	2.00	.26
1.6	.23	.02	.31	.02
1.5	--	--	.03	.003
	(b) 6.0 V at power supply			
1.7	1.43	.46	1.96	.26
1.6	.24	.02	.32	.02
1.5	--	--	.03	.003

LIST OF REFERENCES

1. Nussberger, A., The Final Proceedings of the Solar Power Satellite Program Review, NASA, July 1980.

2. Larin, F., Radiation Effects in Semiconductor Devices, John Wiley and Sons, 1968.

3. Schade, H., Neuse, C.J., and Herrick, D., J. Applied Phys., 41, 3783, 1970.

4. Stanley, A.G., IEEE Trans. Nucl. Sci., NS-17, 239, 1970.

5. Millea, M.F., and Aukerman, L.W., J. Appl. Phys., 5, 168, 1965.

6. Millea, M.F. and Aukerman, L.W., J. Appl. Phys., 36, 2585, 1965.

7. Barnes, C.E., IEEE Trans. Nucl. Sci., NS-18, 322, 1971.

8. Rose, B.H., and Barnes, C.E., J. Appl. Phys., 53, 1772, 1982.

9. Gage, S., et. al., Optoelectronics Applications Manual, McGraw-Hill, 1977.

10. Rudie, N.J., Principles and Techniques of Radiation Hardening, Vol. I, Western Periodicals, 1976.

11. Walt, M., The Trapped Radiation Handbook, Defense Nuclear Agency, 1971.

12. Barnett, M.T. and Cunneen, W.J., Design and Performance of the Electron Linear Accelerator at the U.S. Naval Postgraduate School, Master's Thesis, Naval Postgraduate School, Monterey, California, 1966.

13. Berger, M.J. and Seltzer, S.M., Tables of Energy Losses and Ranges of Electrons and Positions, NASA, 1964.

14. Muller, R.S. and Kamins, T.I., Device Electronics for Integrated Circuits, John Wiley and Sons, 1977.

15. Sze, S.M., Physics of Semiconductor Devices, John Wiley and Sons, 1981.

16. Hardwick, W.H. and Kalma, A.H., IEEE Trans. on Nucl. Sci., 26, 4808, 1979.

AD-A154 441 ELECTRON IRRADIATION OF LIGHT EMITTING DIODES(U) NAVAL POSTGRADUATE SCHOOL MONTEREY CA C Q NESS DEC 84 2/2

UNCLASSIFIED F/G 9/1 NL

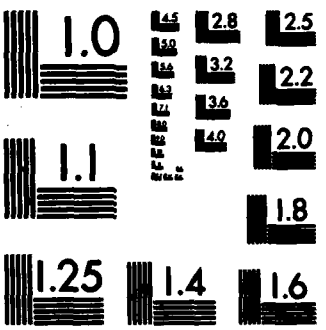

MICROCOPY RESOLUTION TEST CHART
NATIONAL BUREAU OF STANDARDS-1963-A

INITIAL DISTRIBUTION LIST

		No. Copies
1.	Library, Code 0142 Naval Postgraduate School Monterey, California 93943	2
2.	Defense Technical Information Center Cameron Station Alexandria, Virginia 22314	2
3.	Prof. K. C. Dimiduk, Code 61Dm Department of Physics Naval Postgraduate School Monterey, California 93943	10
4.	Prof. H. Handler, Code 61Hr Department of Physics Naval Postgraduate School Monterey, California 93943	1
5.	LCDR C. Q. Ness 19231 Beckford Pl. Northridge, California 91324	3
6.	CDR D. O. Ness, USN (Ret.) 19231 Beckford Pl. Northridge, California 91324	1
7.	Professor K. Woehler, Code 61Wb Department of Physics Naval Postgraduate School Monterey, California 93943	1
8.	D. Snyder, Code 61 Department of Physics Naval Postgraduate School Monterey, California 93943	1

END

FILMED

6-85

DTIC